Charles University in Prague
Faculty of Mathematics and Physics

MASTER THESIS

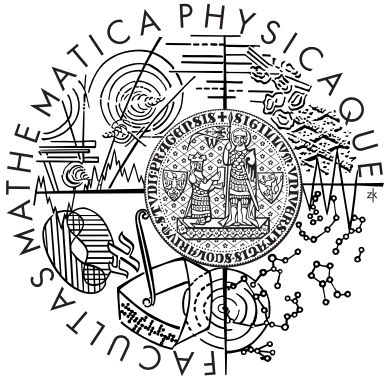

Martina Pagáčová

Time resolution of TileCal and searches for heavy metastable particles

Institute of particle and nuclear physics

Supervisor of the master thesis:	doc. RNDr. Rupert Leitner, DrSc.
Co-supervisor of the master thesis:	RNDr. Tomáš Davídek, Ph.D.
Study programme:	Physics
Specialization:	Nuclear and subnuclear physics

Prague 2012

I would like to express my big gratitude to my diploma supervisor doc. RNDr. Rupert Leitner, DrSc. and co-supervisor RNDr. Tomáš Davídek, Ph.D. for their careful guidance and valued feedback. My great acknowledgments belong also to Antonella Succurro for her help with data analysis. Last, but not least, I would like to express my special thanks to my parents, sister and partner for their great patience, support and care.

I declare that I carried out this master thesis independently, and only with the cited sources, literature and other professional sources.

I understand that my work relates to the rights and obligations under the Act No. 121/2000 Coll., the Copyright Act, as amended, in particular the fact that the Charles University in Prague has the right to conclude a license agreement on the use of this work as a school work pursuant to Section 60 paragraph 1 of the Copyright Act.

Prague, 12th April 2012 Martina Pagáčová

Contents

Název práce: Časové rozlíšenie TileCalu a hľadanie ťažkých metastabilných častíc
Autor: Martina Pagáčová
Ústav: Ústav časticové a jaderné fyziky
Vedoucí diplomové práce: doc. RNDr. Rupert Leitner, DrSc.
E-mail vedoucího: Rupert.Leitner@cern.ch

Abstrakt: Predložená práca sa zaoberá štúdiom časovania kalorimetru TileCal experimentu ATLAS prostredníctvom dát single hadrónov. Časové rozlíšenie rovnako ako odozva stredného času závisia na deponovanej energii v danej cele. Výsledky sú porovnané s predchádzajúcimi analýzami s jetmi a miónami. Presné meranie doby letu pomocou TileCalu môže identifikovať ťažké dlhožijúce častice, ktoré sú predpovedané modelmi za štandardným modelom. Ich hmotu je možné zrekonštruovať skombinovaním tohto merania s meraním hybnosti vo vnútornom detektore experimentu ATLAS. Nakoniec je vypočítaná chyba určenia hmoty exotickej častice o hmotnosti $M = 600$ GeV.

Klíčová slova: ATLAS experiment, TileCal kalorimeter, časové rozlíšenie, stabilné ťažké častice

Title: Time resolution of TileCal and searches for heavy metastable particles
Author: Martina Pagáčová
Department: Institute of Particle and Nuclear Physics
Supervisor: Doc. RNDr. Rupert Leitner, DrSc.
Supervisor's e-mail address: Rupert.Leitner@cern.ch

Abstract: In the present work, the timing of the ATLAS TileCal is studied using the single hadron collision data. The time resolution and also the mean time response depend on the energy deposited in a given cell. The results are compared to the previous analysis with jets and muons. Precise time-of-flight measurement using TileCal can be used to identify the heavy long-lived particles predicted by the models of physics beyond the standard model. Their mass can be reconstructed by combining with the momentum measurement in the ATLAS inner detector. Finally, the mass resolution of an exotic particle with mass $M = 600$ GeV is estimated.

Keywords: ATLAS experiment, TileCal, time resolution, stable massive particles

Chapter 1

The ATLAS experiment

1.1 The Large Hadron Collider

The Large Hadron Collider (LHC) is a synchrotron located at the European Organization for Nuclear Research (CERN) in the northwest suburbs of Geneva on the Franco-Swiss border. It is designed to collide opposing particle beams of either protons or heavy ions. Since March 2010, the LHC operates at the center-of-mass energy 7 TeV and will reach up to 14 TeV. Therefore when completed, it will be the largest and at the same time the most energetic particle accelerator in the world. The designed luminosity of the LHC is $10^{34}\text{cm}^{-2}\text{s}^{-1}$ [1] and the nominal LHC bunch-crossing period is 25 ns. There will be about 23 interactions per bunch crossing at the designed luminosity.

The LHC is the first collider whose energy and luminosity is high enough to probe the physics at the TeV scale. Ergo, some theoretical scenarios beyond the Standard Model can be verified or disapproved.

1.2 The ATLAS detector

The ATLAS (A Toroidal LHC Apparatus) detector is one of the four main LHC experiments. It is a general purpose detector designed to explore a wide range of physics processes at the LHC. This experiment measures with high precision the parameters of the Standard Model (SM)[1] and has also a great discovery potential of new phenomena beyond the SM.

[1]The Standard Model of elementary particles and their interactions is the theory of the particle physics that describes the electromagnetic, weak and strong interactions between elementary particles.

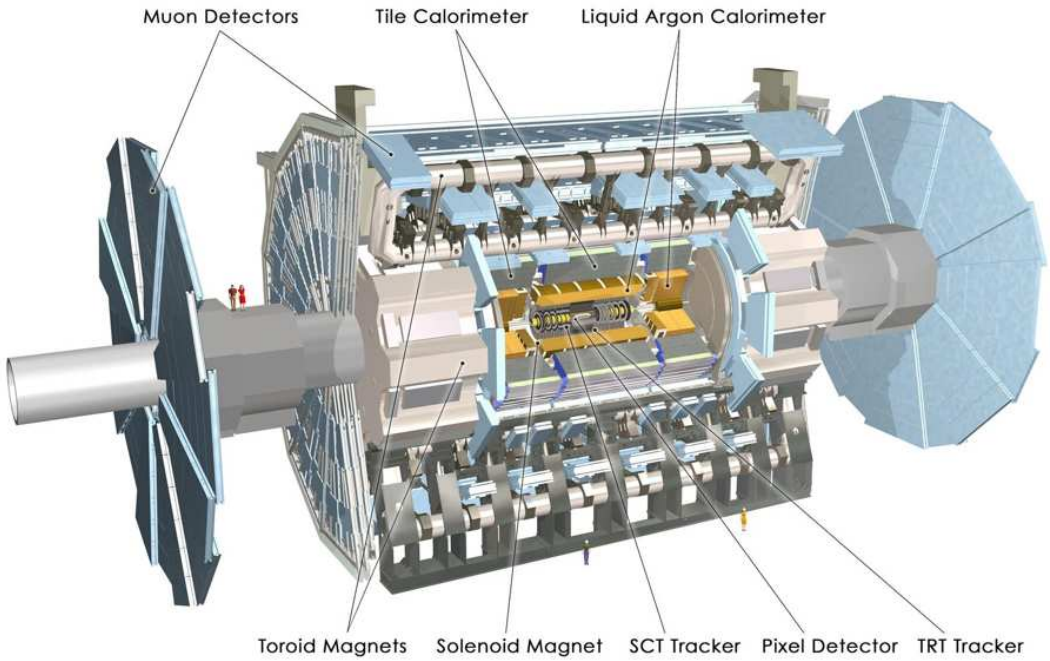

Figure 1.1: The ATLAS detector [1]

Figure 1.1 shows a three dimensional illustration of ATLAS detector. It is forward-backward symmetric with respect to the interaction point. The ATLAS detector is 44 meters long and 22 meters in diameter with weight about 7000 tons. In order to identify all particles produced at the interaction point where the particle beams collide, particle detectors are usually designed with three different detecting subsystems: Inner Detector, Calorimetry and Muon spectrometer. Each subdetector specializes in measuring different characteristics of the particles that can serve as a tool for their detection and identification. They are briefly described in the next section.

1.2.1 ATLAS coordinate system

The coordinate system of ATLAS is a right-handed system with the origin in the interaction point. The z axis is defined as the beam axis and the plane transverse to the beam line is xy plane. The x axis points to the center of the LHC tunnel and z axis points upwards. The azimuthal angle ϕ is measured from the positive x axis and increases clockwise looking in the positive z direction. The polar angle θ is the angle relative to the beam direction.

Another important parameters to describe the particles inside the ATLAS detector are p_T and η where p_T is the transverse momentum i.e. the momentum in the xy plane and η is the pseudorapidity of particles from the primary vertex defined as:

$$\eta = -\ln \tan\left(\frac{\theta}{2}\right) \tag{1.1}$$

Distance between particles in $\eta - \phi$ space is described by a so-called cone size ΔR:

$$\Delta R = \sqrt{\Delta\eta^2 + \Delta\phi^2} \tag{1.2}$$

1.2.2 Inner Detector

The subdetector located the closest to the interaction point is the Inner Detector. It covers the region of pseudorapidities $|\eta| < 2.5$. Its main purpose is the trajectory reconstruction and the momentum measurement of charged particles. Therefore, it is wholly immersed in a 2 T solenoidal magnetic field. The position of the detector induces the great occupancy and diversity of the particles. Hence, the high granularity is required for isolation of a single track. Moreover, it has to be very fast to cope with the 40 MHz bunch crossing frequency. The Inner Detector consists of three different parts: the Pixel Detector, the Semi-Conductor Tracker (SCT) and the Transition Radiation Tracker (TRT).

The Pixel Detector

The pixel detector is the innermost component of the whole ATLAS experiment. Its smallest units are square pixels of 400 μm along the z-axis and 50 μm in the xy-plane, each working as diodes driven in a reverse-bias mode. Typically each track crosses three pixel layers. In total, there are about 80 millions pixels providing good spatial resolution and exact vertex reconstruction. In the xy plane i.e. the bending plane of the magnetic field, the position is measured with excellent 12 μm precision. While in the z direction, the spatial resolution is about $66 - 77$ μm.

The Semi-Conductor Tracker (SCT)

The SCT represents the precision tracking detector consisting of the long narrow silicon strips, 80μm$\times$12cm in size. The system is composed of four concentric double layers designed to provide eight measurements per track in the intermediate radial range. The spatial accuracies are 17 μm in $R\phi$ and 580 μm in the z direction. The number of readout channels is approximately 6.3 million.

The Transition Radiation Tracker (TRT)

The TRT is the outermost layer of the Inner Detector composed of straw tubes with a diameter of 4 mm. These drift chambers are filled with a xenon mixture. This allows the electron identification via the transition radiation. The intrinsic accuracy is 170 μm per straw. However the detector provides a large number of measurements per track, typically 36. The combined resolution is thus better than 50 μm. The total number of TRT readout channels is approximately 351 000.

1.2.3 Calorimetry

The ATLAS calorimeter system has been designed to reconstruct the energy of electrons, photons and jet, as well as to ensure a good measurement of the missing transverse energy E_T^{miss}. It consists of two sampling detectors with full ϕ-symmetry: an inner electromagnetic calorimeters and an outer hadronic calorimeters.

The electromagnetic calorimeter (ECAL)

The electromagnetic calorimeter is a lead/liquid argon (LAr) detector consisting of a barrel ($|\eta|$ <1.475) and two end-caps (1.375< $|\eta|$ < 3.2) housed in three cryostats. It identifies the electrons, positrons and photons and measures with high accuracy their energy and position. The ECAL uses accordion-shaped absorbers and kapton electrodes which collect the charge of ionization electrons. This structure provides complete ϕ symmetry without azimuthal cracks. The total thickness of the detector is $> 24\ X_0$ (radiation lengths) in the barrel and $> 26\ X_0$ in the end-caps with approximately 190 000 readout channels.

The hadronic calorimeter (HCAL)

The main function of HCAL is to identify and reconstruct jets as well as to measure their energy loss and thus the missing transverse energy E_T^{miss}. The last mentioned is the energy carried away by non-interacting particles (e.g. neutrinos in the Standard Model) and is very important for many exploitable channels, in particular for SUSY particle searches. The system consists of two different detector technologies: the Tile technology in the barrel part (Tile Calorimeter) see Section 2.1 and the LAr technology in the hadronic end-cap (HEC) and forward region (FCal). The Tile Calorimeter is a steel/plastic scintillator plates detector covering the pseudorapidity range of $|\eta| < 1.7$. It operates at room temperature. At larger pseudorapidities, where higher radiation resistance is needed, the liquid-argon detectors are used. The range $1.5 < |\eta| < 3.2$ is covered by the HEC, while the FCal is used in the region $3.1 < |\eta| < 4.9$. Both are housed in the same cryostat together with the EM end-caps.

1.2.4 Muon Spectrometer

The muon spectrometer is the outermost and also the largest by volume component of the ATLAS detector. It was designed to measure the deflection of muon tracks in the superconducting air-core toroid magnets up to $|\eta| <2.7$ and to trigger on them in the range $|\eta| < 2.4$. Over most of the pseudorapidity range, the high-precision tracking is provided by Monitored Drift Tubes (MDTs). At large pseudorapidities and closer to the interaction point, Cathode Strip Chambers (CSCs) with higher granularity are used. The toroidal field bends the track in polar angle θ while the solenoidal field in the inner detector curves the particles in azimuthal angle ϕ. Therefore, the standalone momentum measurement is made in $R - z$ projection. The z coordinate is measured in the barrel ($|\eta| < 1$) while the R coordinate in the transition ($1.0 < |\eta| < 1.4$) and end-cap regions ($1.4 < |\eta| < 2.7$).

1.2.5 Trigger System

The ATLAS trigger system consists of three levels of online event selection: Level-1 (L1), Level-2 (L2), and Event Filter. The Level-2 and the Event Filter, making up the High-Level Trigger, are implemented entirely in software, while the Level-1 operates with custom-made electronics i.e. runs at the hardware level.

Its purpose is to reduce the initial bunch-crossing rate of 40 MHz to about 100 Hz for permanent storage and following analysis. The L1 trigger exploits the calorimeter system and muon detectors with reduced granularity information to make an initial selection. It searches for high p_T muons, electrons/photons, jets, $\tau-$leptons decaying into hadrons and large E_T^{miss}. The L1 accept rate is approximately 75 kHz within the decision time less than 2.5 μs. The L2 trigger can use full-granularity data from all detectors and combine the information from different subdetectors. It reduces the event rate below 3.5 kHz. The processing time is 10 ms in average. Afterwards, the full event is sent to the Event Filter which is based on the offline analysis procedure. The output event rate to be recorded for the offline analysis is about 100 Hz. This corresponds to an output data rate of 100 MB/s.

Chapter 2

The Tile Calorimeter

The Tile Calorimeter (TileCal) is a hadronic calorimeter located in the central region of the ATLAS detector. It is a hadronic sampling calorimeter using steel as the absorber material and plastic scintillating tiles as the active medium. Its main task is to identify jets and measure their energy and position, as well as to provide the precise measurement of the time of flight of all particles crossing it. This chapter will review the basic description of the detector, followed by a detailed explanation of the signal reconstruction and ending with the calibration concept.

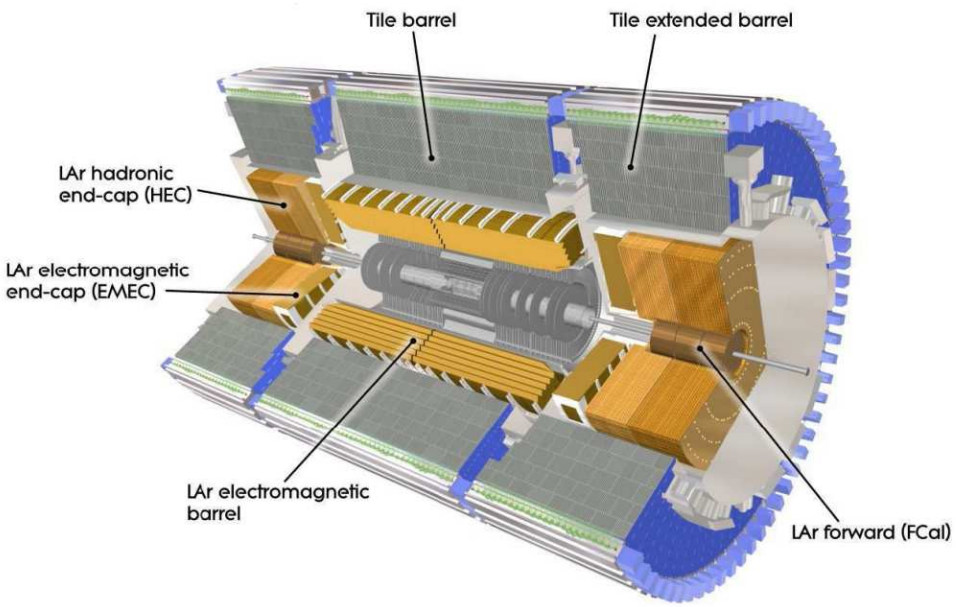

Figure 2.1: The Calorimeter system [2]

2.1 Tile Calorimeter description

2.1.1 Mechanics

The TileCal passive absorber builds up a steel matrix containing the scintillating tiles at periodic intervals. This structure is connected to a massive element, referred to as a girder, which is placed at the outer radius of the calorimeter. It is the structural support of the module which houses the readout electronics. Moreover, its cross section is sufficient to provide the flux return for the solenoidal field.

The subdetector is mechanically composed of three cylindrical sections called barrels. The 5640 mm long barrel (LB) covers the central part of the detector ($|\eta| < 1.0$) and the two 2910 mm extended barrels (EB) flank the detector on both sides ($0.8 < |\eta| < 1.7$). The TileCal is symmetric with respect to the beam line as well as the direction $\eta = 0$ (Figure 2.1).

In the gap between the barrel and extended barrel parts, there is a stepped calorimeter structure called Intermediate Tile Calorimeter (ITC). Its configuration tries to maximize the volume of active medium and simultaneously leaving enough space for the Inner Detector and Liquid Argon cables and services. The ITC consists of a calorimeter plug in the region $0.8 < |\eta| < 1.0$ and bare scintillators in $1.0 < |\eta| < 1.6$. These scintillators are then divided into gap scintillators ($1.0 < |\eta| < 1.2$) and crack scintillators ($1.2 < |\eta| < 1.6$). In the present configuration, the TileCal readout includes also the Minimum Bias Trigger Scintillators (MBTS) which are installed on the front face of the end-cap calorimeter cryostats and are used to trigger on minimum bias events and to identify the beam background. The MBTS, located in the $2.1 < |\eta| < 3.8$, are designed to function only during the low-luminosity running because of the radiation damage.

Each barrel is segmented azimuthally into 64 sectors, referred to as modules (Figure 2.2), corresponding to a $\Delta\phi$ granularity of ~ 0.1 radians ($\Delta\phi = 2\pi/64 \sim 0.1$). Radially, the Tile Calorimeter extends from an inner radius of 2280 mm to an outer radius of 4230 mm. It is longitudinally divided into three different layers. These layers are called A, BC and D and at the pseudorapidity $\eta = 0$ they are approximately 1.5, 4.1 and 1.8 λ_{int} (nuclear interaction length for protons) thick for the barrel and 1.5, 2.6 and 3.3 λ_{int} for the extended barrel, respectively.

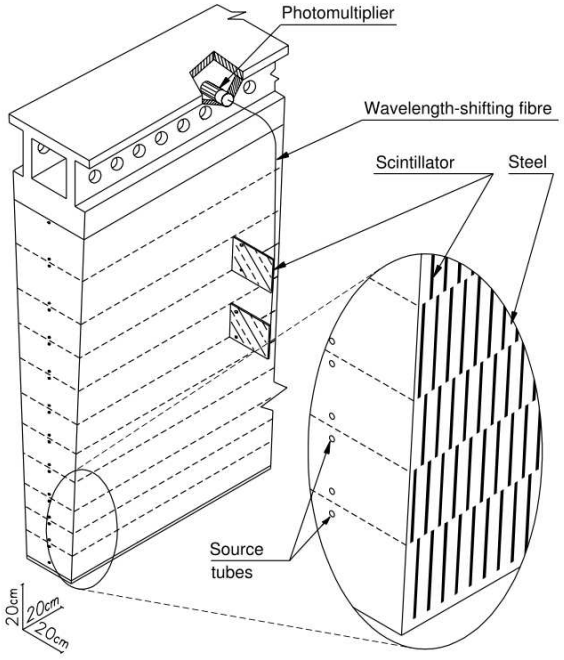

Figure 2.2: The TileCal module structure, showing the scintillating plastic tiles embedded in a steel matrix and the principle of light collection by WLS fibers to PMTs [2].

2.1.2 Optics

The charged particles produced in a hadronic shower induce an emission of ultraviolet scintillating light in the scintillating tiles which is collected and consequently converted to visible light by wavelength shifting (WLS) fibers running radially along the two outside sides of each module. This optical instrumentation is thus independent from the mechanical assembly which leads to the design simplicity and the cost-effectiveness. By grouping together a set of WLS fibers into a photomultiplier (PMT), a 3D read-out cell geometry is defined and projective η tower structure is created for the energy and trigger reconstruction (Figure 2.3). The resulting typical cell dimensions are $\Delta\phi \times \Delta\eta = 0.1 \times 0.1$ (in the layers A and BC) and $\Delta\phi \times \Delta\eta = 0.1 \times 0.2$ (in the layer D).

The scintillating tiles lie in the $r - \phi$ plane and are radially staggered in depth. There are 11 different sizes of tiles with trapezoidal shape. Their azimuthal dimension varies from 200 to 400 mm and the radial one from 100 to 200 mm, though the thickness is always 3 mm. In order to fill the

whole calorimeter, approximately 460 000 tiles are required. The iron to scintillator ratio is 4.67:1 by volume [3]. The particularity of this subdetector is that these scintillating plates are placed perpendicularly to the beam axis. This is a new technology which allows simpler readout and tile configuration because the electronics can be located at the top of each module. However, the inconvenience of this structure is a strong dependence of the sampling fraction at the pseudorapidity η, especially close to $\eta = 0$.

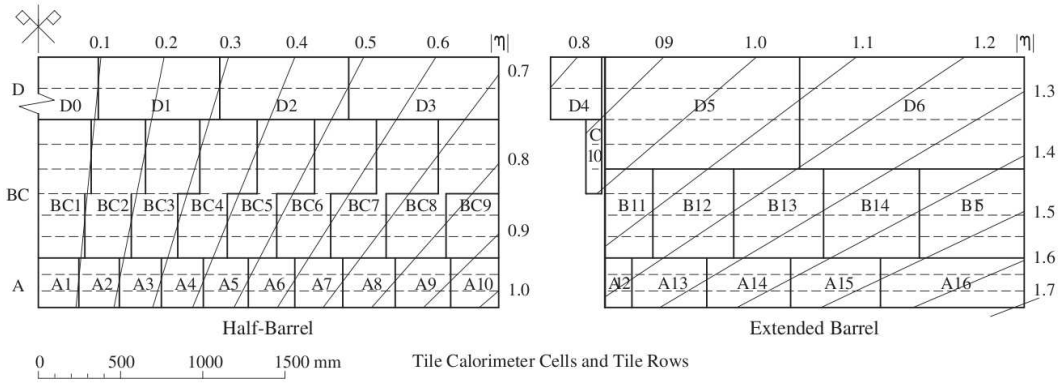

Figure 2.3: TileCal cells and tile-rows distribution of half central barrel (on the left), extended barrel (on the right) and ITC (cells D4 and C10). Horizontal dashed lines show the 11 rows of scintillating tiles and solid lines the cell boundaries. Lines of fixed pseudorapidity η are also drawn [2].

2.1.3 Electronics and readout

The overall design of the TileCal readout is rather simple and compact. Its full chain from the light signal to the digital data is shown in Figure 2.4 [4].

The front-end and digitizing electronics are mounted inside the removable 3 m long superdrawer which is situated inside the girder in the backbeam region of the calorimeter module. Each superdrawer is composed of two physical drawers which are coupled from the electronics point of view. In total there are 256 superdrawers, one for each external barrel module and one for each half central barrel module. Therefore, the TileCal is divided by the readout architecture in four electronically independent partitions: LBA, LBC (long barrel), EBA and EBC (extended barrels)[2]. The super-

[2]A correspond to the Anti-clockwise direction of the beam line (positive pseudorapid-

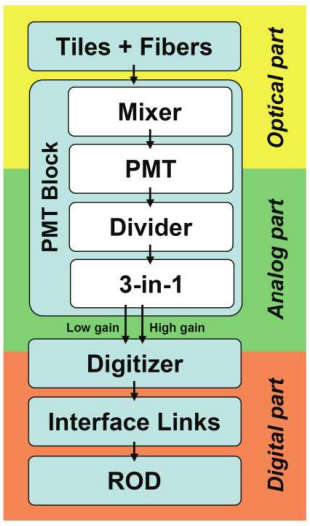

Figure 2.4: Scheme of TileCal readout

drawer contains 45/32 photomultipliers (PMTs) in the barrel/extended barrel. Each PMT is linked to one readout channel. The absolute number of the channels, cells and trigger outputs is summarized in Table 2.1.

	Channels	**Cells**	**Trigger outputs**
Long barrel	5760	2880	1152
Extended barrel	3564	1790	768
Gap and crack	480	480	128
MBTS	32	32	32
Total	9836	5182	2080

Table 2.1: Number of channels, cells and trigger outputs of the TileCal: LB, EB, gap, crack and MBTS (the channels of last three parts are readout in the EB drawers) [2]

The front-end electronics of each superdrawer consists of 4 subsystems, as seen in Figure 2.5:

(1) 45/32 PMT blocks in barrel/extended barrel
(2) 4 Motherboards
(3) 8/6 Digitizer boards in barrel/extended barrel
(4) 1 Optical interface board

ity) and C to the Clockwise direction (negative pseudorapidity)

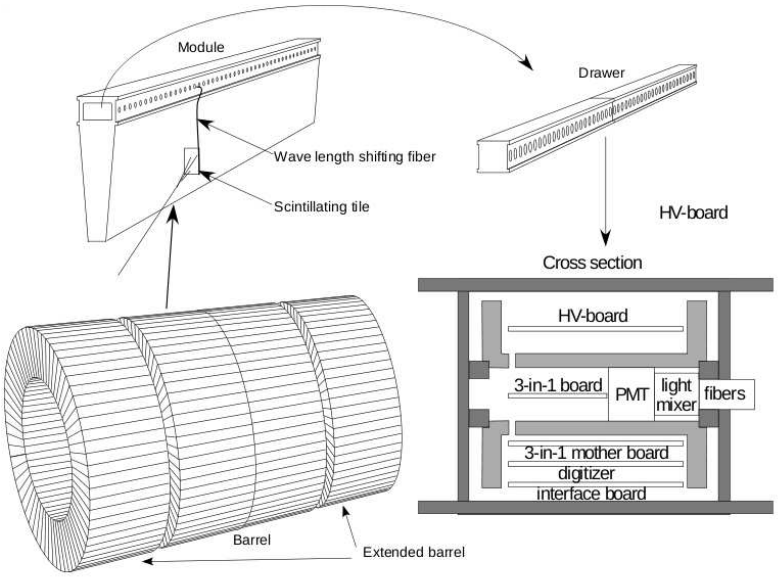

Figure 2.5: Scheme of TileCal, its wedge-shaped modules with removable drawers and a cross section of a drawer [5]

PMT block

A PMT block, located in dedicated hole inside a drawer, is designed to convert light into electric signals. It contains a PMT, a light mixer, a HV divider and a 3-in-1 card, all inserted in a steel cylinder in order to provide magnetic shielding. The light mixer ensures the interface between the PMT and the fiber bundle. The HV divider distributes the high voltage between the dynodes of the PMT. The 3-in-1 card assures three following functions: fast PMT pulse shaping and amplification, charge injection calibration and slow PMT signal integration. The last two are designed to calibrate the readout electronics. The first one converts a PMT signal ($\sim$ 18ns FWHM[3] with a 5ns rise time) into a pulse which is suitable for the fast ADC and can be subsequently transmitted to the fast digitizers. The input signal to the ADC has 50 ns FWHM with an amplitude proportional to the input charge i.e. to the energy deposited in a channel. Hence, the 3-in-1 card has four signal outputs: one for Level-1 trigger, one for calibration purpose and two linear outputs to the Digitizer board [6]. The outputs referred to as low and high gain pulses have a relative gain of 64.

[3]FWHM states for the acronym of full-width at half-maximum.

Digitizer board

A superdrawer holds 8 Digitizer boards in a central barrel and 6 in an external barrel, each serving 6 readout channels. It is at this level that the analogue signal coming from the PMTs via the 3-in-1 cards is sampled and digitized. A scheme with a double readout using two independent 10-bit ADCs was chosen to cover a 16 bit dynamic range i.e. to measure the particle energies, extending from typical muon energy deposition (a few hundreds of MeV) to energetic jet deposition (up to 2 TeV) in a single cell. In one Digitizer card, there are thus twelve 10-bit ADCs in order to digitize the pulse from 6 channels with two gains. The gain is chosen automatically. The analog data are sampled each 25 ns, typically 7 times in physics mode and up to 9 times for calibration purposes. The samples are then processed by a so-called TileDMU (Data Management Unit) chip which stores them in a local pipeline memory during around 2.5 μs until L1 trigger takes the decision. If the event is accepted, the string of digital samples is sent to the interface card.

Besides the ADCs, each Digitizer board is equipped with two TileDMUs, the TTC receiver and decoder chip (TTCrx). The ATLAS Timing, Trigger and Control (TTC) system is an optical fiber based system which distributes especially the trigger accepts and the 40 MHz system clock which is synchronized with the LHC bunch-crossing frequency. The TTC receiver chip (TTCrx) is an interface between the TTC optical system and the front-end electronics [6]. It receives the system clock and distributes the sampling clock, called `clock40des2`, to the Digitizer boards. The `clock40des2` clock determines when the sampling of the ADC input signal should start. It is also a 40 MHz clock but can be delayed in order to compensate for particle times of flight and for propagation delays associated with the detectors and their electronics [8]. The delay, referred to as `dskew2`, is programmable in multiples of $\sim$ 0.1 ns up to 25 ns and allows to adjust the phase between the sampling clock and the physical pulse.

Interface board

Each superdrawer contains only one this optoelectronic Interface card. It has four main tasks [7]. First, it receives the TTC optical information which is then decoded (converted into electrical signal) by the TTCrx chip and subsequently distributed to the 8 Digitizer boards. Second, it collects the digital samples coming from the Digitizer card. Third, the data is aligned and sorted into event frames. Forth, it transmits data over optical links to the back-end electronics, the readout driver (ROD).

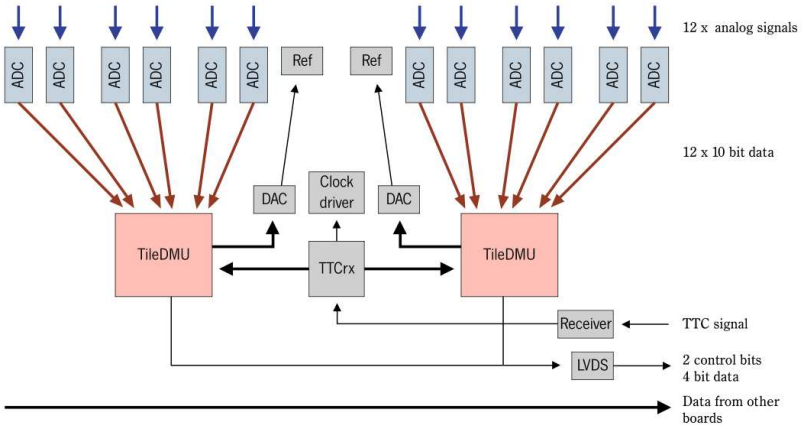

Figure 2.6: Scheme of Digitizer board [9]

2.2 Calibration and monitoring

The main purpose of the Tile Calorimeter monitoring and calibration system is to establish, monitor and correct the reference detector response. As a signal path can be divided into the optical part (the scintillating tiles and the WLS fibers), the PMT and the readout electronics, a dedicated calibration system was designed for each of these sections independently:

(1) Cs radioactive source system for calibrating the optical part and PMTs
(2) Laser system for calibrating the PMTs gain and the electronics
(3) Charge Injection System (CIS) for calibrating the digital system
(4) Minimum Bias (MB) monitoring system for monitoring all TileCal

2.2.1 Cesium calibration

The cesium calibration system is used as the primary tool to determine the quality of the optical response of each TileCal cell and to adjust the PMT high voltage in order to equalize the response from all cells. It uses a hydraulic system to move a ^{137}Cs γ source ($E_\gamma = 662$ keV) through the holes in every scintillating tile and absorber plate. An absorption length of such photons is ~ 1.9 cm in iron and much more in scintillator i.e. the mean free path is comparable to the periodic 18 mm separation between tiles. Therefore, the response of individual tiles can be clearly seen. The current signal from each PMT is read out by the integrator circuit located on the 3-in-1 cards.

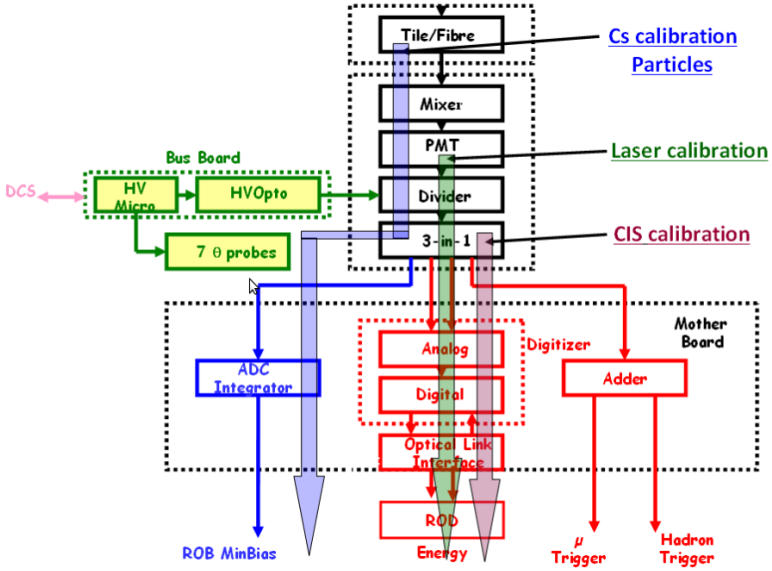

Figure 2.7: Calibration schema in the Tile Calorimeter [14]

2.2.2 Laser system

The laser system is designed to calibrate and monitor the response of the PMTs with an accuracy better than 0.5% [10]. It is also used to map the individual PMT nonlinearities, to study the pulse saturation and can also be used for timing synchronization of the read-out channels. The system produces pulses with a wavelength of 532 nm and a 10 ns width, synchronized with the LHC bunch-crossing clock that are sent to all TileCal PMTs using an optical fiber distribution system. It provides calibration constants for the gain non-linearity and stability in time of the PMTs. The contribution of the laser calibration to the TileCal timing is important for this thesis, therefore it will be described in more details in next chapter.

2.2.3 Charge injection system

The CIS system is located on the 3-in-1 card and is designed for the calibration of the Analog to Digital Converters (ADCs). It injects well defined charge into fast bi-gain electronics and after the pulse is reconstructed from ADC samples, using the Fit Method (see Section 3.1.2), a calibration factor $C_{ADC \to pC}$ can be extracted. These conversion constants are calculated for each individual channel with the systematic uncertainty of $\pm 0.7\%$.

2.2.4 Minimum bias monitoring system

The minimum bias (MB) events in ATLAS are inelastic pp collisions with low momentum transfer, whose rate is proportional to the LHC luminosity. They produce a significant signal in the TileCal cells, with rates uniform in the azimuthal angle ϕ and moderately dependent on the pseudo-rapidity η. In addition to the intrinsic noise, the MB events are one of the limits on the TileCal performance. However, thanks to the features of the MB signal it can be used to detect relative variations in time in the response of the individual cells. Moreover, as the system can operate during the collision data taking it plays complementary roles to the cesium calibration system. Both mentioned calibration systems have the integrator readout path.

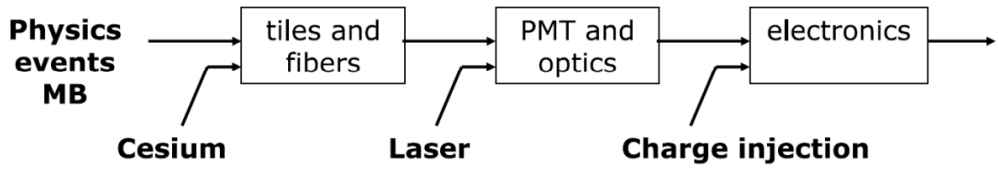

Figure 2.8: Diagram of the optical and electronic readout, and of the calibration and monitoring systems [16].

Chapter 3

Signal reconstruction

The output of the front-end electronics contains the information from each TileCal readout cell, specifically the energy deposited by a particle and the arrival time of the signal. In order to convert the string of digital samples into these physical quantities three different signal reconstruction methods have been developed: the Fit method and the Optimal Filtering algorithm. They are described in the following section.

3.1 Digital signal reconstruction algorithms

3.1.1 Fit method

This method was developed during the testbeam and used until the ROD installation. Nowadays, only the CIS calibration data are reconstructed with this method. It uses the knowledge of the pulse shape from the front-end electronics in order to reduce the contribution of the electronics noise to the energy measurement and to determine the timing of the energy deposition. For each channel/PMT a fit is performed to the data with the function:

$$f(t) = Ag(t - \tau) + ped \tag{3.1}$$

where A (amplitude), τ (phase), ped (pedestal i.e. electronic noise) are three signal parameters that have to be determined. A given function g represents the expected shape of the signal at the output of the 3-in-1 card schematically shown in Figure 3.1 and is quite insensitive to the amount of deposited energy. This method is not suitable for fast online signal processing.

3.1.2 Optimal Filtering algorithm

The optimal filtering (OF) algorithm reconstructs the signal using a weighted sum of the digital samples. Due to the simplicity of this mathematical formulation, its application is fast. Therefore the OF is implemented in the Digital Signal Processors (DSPs) of the TileCal RODs and provides the reconstruction during the online data-taking. In addition to the energy and time, it allows to estimate also the quality of the reconstruction. The procedure to compute these quantities for each PMT is given by the linear combinations of the samples S_i:

$$A = \sum_{i=1}^{N} a_i S_i \tag{3.2}$$

$$\tau = \frac{1}{A} \sum_{i=1}^{N} b_i S_i \tag{3.3}$$

$$ped = \sum_{i=1}^{N} c_i S_i \tag{3.4}$$

$$QF = \sum_{i=1}^{N} \mathrm{abs}(S_i - A g_i) \tag{3.5}$$

where N is the total number of samples, A stands for the amplitude, τ is the phase of the signal and *ped* represents the pedestal. QF is the quality factor of the reconstruction. The values g_i are the amplitudes of the normalized shape function for the i-th sample. The weights a_i, b_i, c_i are obtained from knowledge of the shape and expected time position of the pulse and are chosen in such a way that the variance of the parameters against the electronic noise and Minimum Bias (MB) pile-up fluctuations is minimized [11]. The reconstruction is thus very sensitive to variations in any of these parameters. The weights are calculated offline and downloaded into the DSP at configuration time [13]. The signal reconstructed by the OF has an energy precision of 1% [15]. The reference pulse shape used for the OF weights calculation is shown in the Figure 3.1.

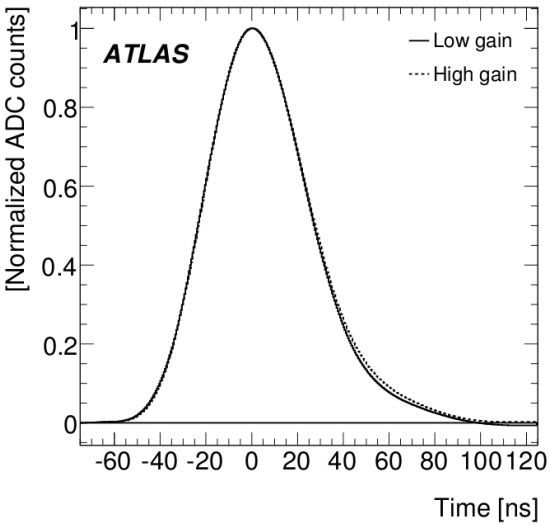

Figure 3.1: Pulse shape for high and low gain used as reference for the estimation of the OF weights [2]

Figure 3.2 represents the final pulse and the definition of its three parameters i.e. the reconstructed quantities. The *pedestal* is defined as the baseline level of the signal. The *phase* is the time difference between the central sample and the pulse maximum (see the next section). The *amplitude*, referred to as the distance between the peak and the pedestal, represents the measured energy in ADC counts. To obtain the channel energy in GeV, the following equation is used [2]:

$$E_{channel} = A \cdot C_{ADC \to pC} \cdot C_{pC \to GeV} \cdot C_{Cs} \cdot C_{Laser} \tag{3.6}$$

where the factor $C_{ADC \to pC}$ is the conversion factor of ADC to charge. For each channel it is defined via a well defined injected charge with the CIS (Charge Injection System) calibration system. The factor $C_{pC \to GeV}$ is the conversion factor of charge to energy in GeV and is determined by measuring signals of electron beams at known energies. The factor C_{Laser} corrects for non-linearities of the PMT response measured by the Laser calibration system and the factor C_{Cs} corrects for residual non-uniformities after the gain equalization obtained from the Cesium Calibration system.

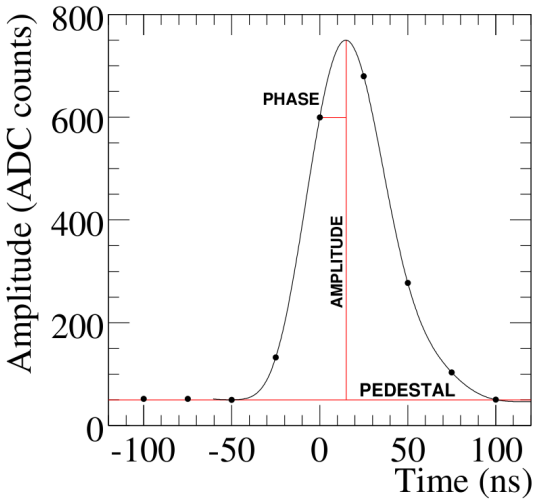

Figure 3.2: Definition of the three OF independent parameters: amplitude, phase and pedestal. The dots correspond to the ADC samples taken every 25 ns [11].

3.2 TileCal timing

The time-of-flight of a particle that deposits energy in the TileCal cell is measured from the interaction point to that cell. As the light from each cell is read out by two PMTs, the cell time is represented by their average. Its precise measurement is important for background removal and also for physics analysis.

At ATLAS, the convention is to compensate for the time-of-flight such that a signal left by a particle traveling at the speed of light ($\beta = 1$) has $t = 0$. All known particles, produced at the high energy pp collisions are relativistic. This setting is then adequate and done for each channel prior to the data taking. The signal is reconstructed using the OF algorithm which is based on the assumption that $\tau = 0$ [4]. In this sense, the arrival time t of a particle is compatible with the phase τ of the reconstructed pulse. The OF method is designed to yield the best performance when the ADC central sample is within 2 ns from the peak of the analogue pulse i.e. within small phase variations. Therefore, the quality of the reconstruction decreases with increasing τ. Firstly, this occurred during the TileCal commissioning with cosmic muons since they cross the detector randomly. Unlike during LHC operation where signals have fixed phases given by LHC bunch crossing,

this data is not synchronized with the 40 MHz system clock. Secondly, it can be the case of exotic nonrelativistic particles ($\beta \ll 1$) with a large time-of-flight. The delayed signal in the TileCal can be used for their detection. In order to search for new physics such as massive long-lived particles, it is necessary to handle also the out-of-time energy depositions . Hence, an iterative procedure has been set up.

However, due to insufficient processing time in the DSP, only non-iterative optimal filtering is currently applied online. The misreconstructions and the out-of-time energy depositions are detected by a poor quality factor QF and consequently allowed for an offline dedicated treatment. Furthermore, the use of non-iterative optimal filtering technique is required in order to minimize all the sources of noise (electronic noise and pile-up).

3.2.1 Iterative OF algorithm

The iterative procedure starts with the estimation of the initial phase τ_0 that determines the index of the maximum sample. It is defined as the time between the central and the maximum sample in units of 25 ns [12]:

$$\tau_0 = 25(i_{central} - i_{max}) \tag{3.7}$$

where i is the index of an appropriate sample. This value is used to compute a new set of OF weights and apply them on the samples in a next iteration. This is repeated until convergence is obtained. The amplitude, phase and pedestal are calculated in each iteration as:

$$A_k = \sum_{i=1}^{N} a_i|_{\tau_{k-1}} S_i \tag{3.8}$$

$$\tau_k = \frac{1}{A_k} \sum_{i=1}^{N} b_i|_{\tau_{k-1}} S_i \tag{3.9}$$

where k is the iteration index and runs from 1 to 3. It is being observed that the three iterations are sufficient to achieve the convergence. If $\tau_0 = 0$ i.e. the maximum sample is the central sample, the first iteration starts with the OF weights obtained using Equations 3.2 and 3.3.

The amplitude reconstructed by the OF method is very sensitive to variation in pulse shape, noise and arrival time of pulse. The red data points on the Figure 3.3 show its underestimation caused by the phase variations. The relative difference between the online non-iterative E_{DSP} and the offline iterative E_{OFL} cell energy reconstruction is plotted versus the cell time t_{DSP} demonstrating the parabolic deviation. This bias can be parameterized and subsequently corrected by applying a factor dependent on the reconstructed signal phase [13]. The blue data points represent the online reconstruction including this phase correction. The average difference between the online and offline reconstruction is within 1% in the window of -10 to 10 ns.

To summarize, two different optimal filtering (OF) methods are imple-

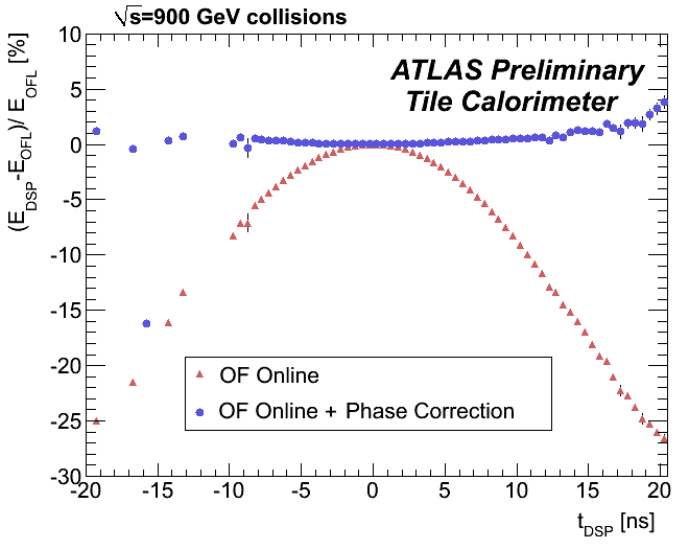

Figure 3.3: Online reconstruction efficiency

mented in the DSP [15]:

(1) *A non-iterative algorithm* (Section 3.1.3) that requires signals to be synchronous within ±2 ns of the digitizing sampling clock (which may be enlarged up to ±10 ns by use of a parabolic correction).

(2) *An iterative algorithm* (Section 3.2.1) which can reconstruct signals that are not synchronous with the LHC bunch crossing (e.g. cosmic muons) and that are delayed up to tens of ns (e.g. massive long-lived particles).

3.2.2 Time calibration

As already mentioned, the phase τ of the reconstructed signal measures the time difference between the fourth[4] sample $t_{4^{th}}$ and the maximum of the reconstructed pulse t_{peak} [6] (Figure 3.4 (a)):

$$\tau \equiv t_{peak} - t_{4^{th}} \tag{3.10}$$

The sign of the phase is interpreted in terms of early or late signal arrival. Since τ must be minimized in order to assure the optimal energy reconstruction by the non-iterative OF method, the condition $|\tau| < 2$ ns should be fulfilled for each channel. Nevertheless, there are a number of especially construction reasons why this does not happen [6]:

(1) The difference of lengths of WLS fibers that collect the light from the scintillating tiles results in the variations of the propagation time in TileCal optics i.e. of the time delays.
(2) The 40 MHz system clock is provided to each digitizer board by the TTC system via TTCrx. The signal enters each drawer via an interface card placed at the center of each barrel drawer and then propagates through adjacent boards on its way through the drawer. The arrival of the system clock to the outermost digitizers is delayed up to 10 ns and the ADC starts sampling the pulse late.
(3) Due to the large size of TileCal, the TTC fibers running from the counting room to each drawer have different lengths. Unlike a short fiber, a long one means the late arrival of the system clock to a drawer. The time difference can be up to 40 ns.

The time calibration of the last two hardware based delays can be achieved using the *laser system*. The time offsets are corrected either by changing the pipeline memory offset Δp in the TileDMUs or by using the `dskew2` in the ADCs. Firstly, the coarse timing adjustment is provided in multiples of 25 ns. The pipeline memory, from which 7 consecutive samples are read out, can be set such that the readout starts one or more samples later or earlier. This programmable setting will be called Δp. Figures 3.4 (b) and (c) show the offsets $\Delta p = -1$ and $\Delta p = +1$, respectively. Secondly, the fine tuning timing is set in units of `dskew2` counts, where 1 count=0.104 ns and maximal 240 counts=25 ns. By finely adjusting the position of the samples, the zero value of the phase τ can be achieved, as seen in the Figure 3.4 (d).

[4]Since TileCal acquires 7 samples in physics mode, the central sample is the 4^{th} one.

These corrections calibrate the front-end electronics digitizers within modules, between modules and between partitions. Although the adjustment of hardware settings is efficient, the accuracy of phase synchronization for individual TileCal channels is limited to be within 3 ns. The reason is that the six channels share the same digitizer board. They are served by one TTCrx, therefore the TTCrx cannot compensate for delays among the channels it is connected to. Moreover, one clock phase is defined for both gains and there is a 2.3 ns difference between their pulse peaks. To calibrate the individual PMTs, the residual time offsets for all channels have to be known with precision. They are remeasured after each modification of the online programmable delays and stored in the TileCal offline database COOL. Consequently, they can be loaded from this database and used as input to the optimal filtering.

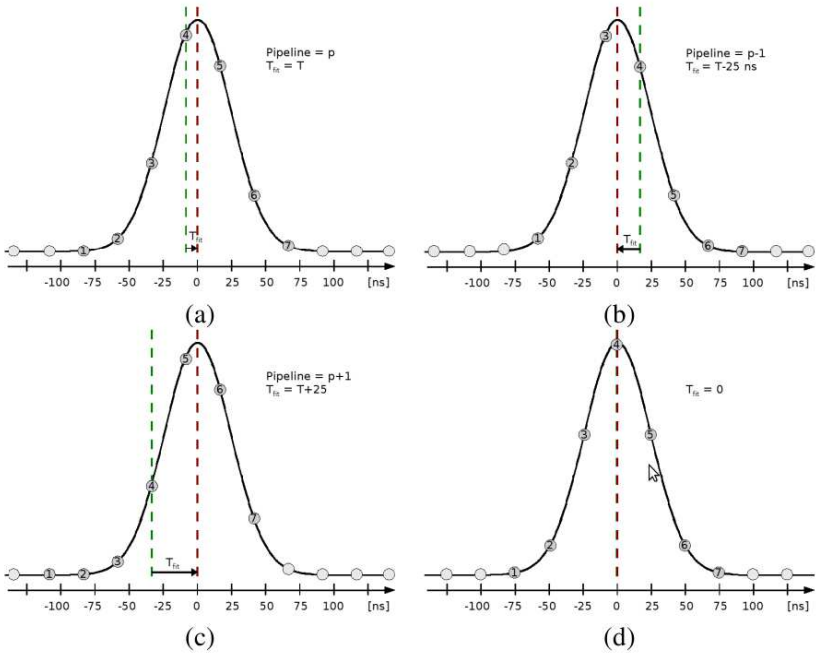

Figure 3.4: Example of both the coarse and fine time adjustments. The numbered circles indicate the samples taken by the ADC and T_{fit} stand for the phase τ.

Some contributions to the time differences are introduced by the laser system itself. The variant lengths of clear fibers, which distribute the laser light are sources of systematic errors in the time offsets. All these corrections to the velocity of propagation of light have been made and accounted for in TileCal database in order to do not degrade the calibration accuracy.

The *single beam data* proved to be very useful in complementing the calibration systems for the synchronization of the calorimeter cells. The timing calibration capability is at the level of 1 ns within a TileCal module and 2 ns within a partition [2]. In particular, the cosmic muon data allows for the opportunity to study the calorimeter response at its full scale. It has thus independently certified the time calibration settings, especially at the second and third layer cell level. In addition, by studying specifically $Z \rightarrow \mu\mu$ events, the cell time spectra were aligned and centered at $t = 0$ [33].

Chapter 4

The TileCal time resolution analysis

The time response of the Tile calorimeter to single charged hadrons (mostly $\pi^{\pm}$), its resolution and the uncertainty of its description by the ATLAS Monte Carlo simulation is discussed in this section. In addition, the results are compared to the analysis with jets and collision muons.

4.1 Event selection

The data used for this analysis has been collected during the 2010 LHC running at a center-of-mass energy of $\sqrt{s} = 7$ TeV. Events have been triggered using the minimum bias trigger scintillators (MBTS) that are, as already mentioned, mounted at each end of the detector in front of the LAr end-cap calorimeter cryostats. The selection of collision candidate events is based on the requirements of at least one reconstructed vertex with at least two associated tracks.

At the calorimeter entrance, a particle starts showering and a cone opens around the extrapolated track. This area of connected energy deposits is identified by the topological clustering algorithm [19]. The cluster energy E_j in the layer j is associated to the track k only if the distance ΔR between the extrapolated track position (η^{kj}_{track},ϕ^{kj}_{track}) and the cluster i position (η^{ij}_{clus},ϕ^{ij}_{clus})[5] is smaller than R_{coll}. This parameter represents the size of a shower. It has been shown that if $R_{coll} = 0.2$ then the energy associated to a track in the minimum bias sample is equivalent to the single pion energy

[5]The location of a cluster is calculated as the energy weighted position of the cells belonging to the cluster.

[17]. Therefore, the following selection has been applied:

$$\Delta R = \sqrt{(\eta^{kj}_{track} - \eta^{ij}_{clus})^2 + (\phi^{kj}_{track} - \phi^{ij}_{clus})^2} < 0.2 \tag{4.1}$$

The sum E of the energies in all the layers j and the energy E^{bad} from the bad cells l in a cluster are then calculated:

$$E = \sum_j E_j \qquad E^{bad} = \sum_l E^{bad}_l \tag{4.2}$$

where a bad cell is a TileCal cell with a bad status e.g. too noisy or not properly calibrated. The track candidate is accepted only if their fraction in absolute value is less than 0.1.

In the case that two tracks are close to each other, the dedicated showers developed in the calorimeter can be superimposed. In order to reduce this shower contamination from charged particles, a search for isolated tracks is performed for each event. The position of each track candidate i is extrapolated to the second longitudinal layer of the electromagnetic calorimeter (η^i_{EM2},ϕ^i_{EM2}). Then, for each of the other track candidates j, the extrapolated position (η^j_{EM2},ϕ^j_{EM2}) is also calculated. If

$$\Delta R_{ij} = \sqrt{(\eta^i_{EM2} - \eta^j_{EM2})^2 + (\phi^i_{EM2} - \phi^j_{EM2})^2} > 0.4 \tag{4.3}$$

for all j, then the track candidate is defined to be isolated [17]. In order to assure that the track is correctly in the calorimeter range, the extrapolated η should satisfy $|\eta_{EM2}| < 2$.

In addition, the isolated tracks coming mainly from hadron decays are often associated with neutral particles. Thus, there is also shower contamination from neutral hadrons and photons (mostly $\pi^0 \to \gamma\gamma$). The idea of the neutral background subtraction is to select charged hadrons that behave like minimum ionizing particles (MIP) in the EM calorimeter [18]. Since this and previous conditions are common for pions and muons, the muon veto has to be applied. Therefore, only the tracks that start showering in the hadronic calorimeter are processed further in the analysis.

Moreover, the high quality isolated track candidates must satisfy the following requirements:

- a transverse track momentum of $p_T > 1.5$ GeV
- a minimum of 1 hit in the Pixel detector and 6 hits in the SCT detector
- small transverse and longitudinal impact parameters computed with respect to the primary vertex, $|d_{0vx}| < 1.5$ mm and $|z_{0vx}| < 1.5$ mm

Finally, after all mentioned event selection criteria are satisfied, a cell selection has to be applied:

- only cells belonging to the reconstructed cluster are considered
- special cells such as D4, C10 and ITC cells, gap and crack scintillators are excluded from the further analysis
- removal of bad-timed cells (careful analysis of the time outliers made by Tomáš Davídek)

4.2 TileCal timing with single hadrons

The TileCal timing performance was studied in several analysis using different datasets: splash events, scraping events, jets in collision and single hadrons from collision. The splash events are produced in the interaction of the LHC beam with the closed collimators, lying 140 meters upstream of the ATLAS detector. These events contain millions of high-energy particles arriving simultaneously in the ATLAS detector. Since the total deposited energy is large, it is only possible to study the timing response in the LG. Scraping events occur when the proton beam hits the edge of the open collimators, allowing a moderate number of particles to the detector [2]. These low-energy deposits are used to study only the HG region. Finally, collision data can monitor the TileCal response in a wide energy range during the data taking. In this section, timing analysis for HG[6] using single hadron collision data is performed.

4.2.1 Time resolution

Each TileCal cell is readout by two PMTs called *e*ven and *o*dd, to which correspond the phases of reconstructed pulses t_e and t_o, respectively. One

[6]Practically no cells in LG.

can consider two variables: $T_1 = (t_e - t_o)/2$ and $T_2 = (t_e + t_o)/2$. The former is the channel time difference and the latter could serve as a measurement of the time of flight of particles with electromagnetic and/or hadronic interactions [20]. Assuming the time synchronization is done accurately, one can integrate over all TileCal cells. These distributions are plotted in a given interval of energies and fitted with a Gaussian function (see Figure 4.1). The value of σ_{T_1} represents an intrinsic time resolution of the TileCal electronics and the signal reconstruction. In order to include all physics factors, the quantity σ_{T_2} has to be used. The Figure 4.2 can serve as an example. The time difference distribution is Gaussian in all energy bins, while the cell time distribution shows a non-Gaussian tail toward positive times at small energies. This effect comes from physics and mirrors the slow hadronic component of the hadronic showers. The tail indeed disappears in muon data [21]. The same is observed in MC time spectra. Both errors would be the same only in case of no correlations between the two time measurements t_e and t_o. At cell level, the correlation is notable as one cell is readout by two channels. However, at reconstruction level, the pulses are reconstructed independently. Altogether, the correlation is not negligible as seen in Figure 4.3.

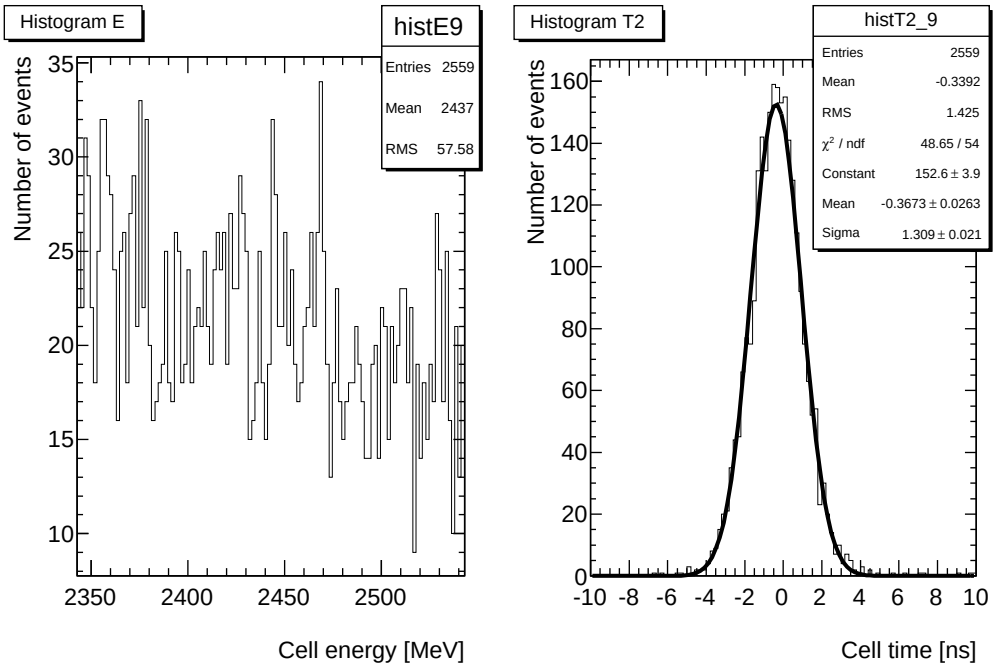

Figure 4.1: Energy and time distribution

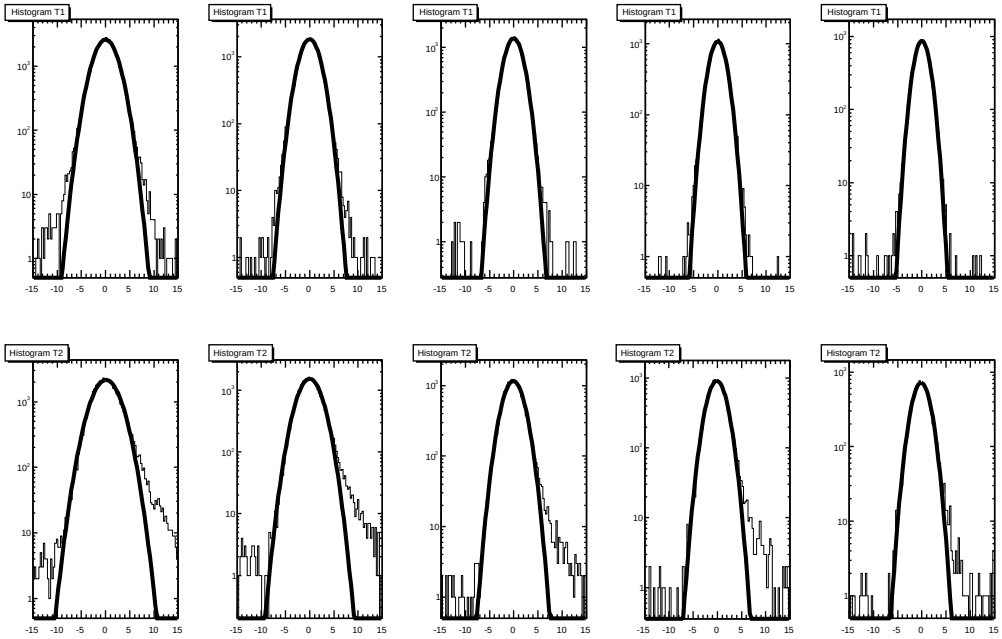

Figure 4.2: Time spectra of T_1 and T_2 in a logarithmic scale

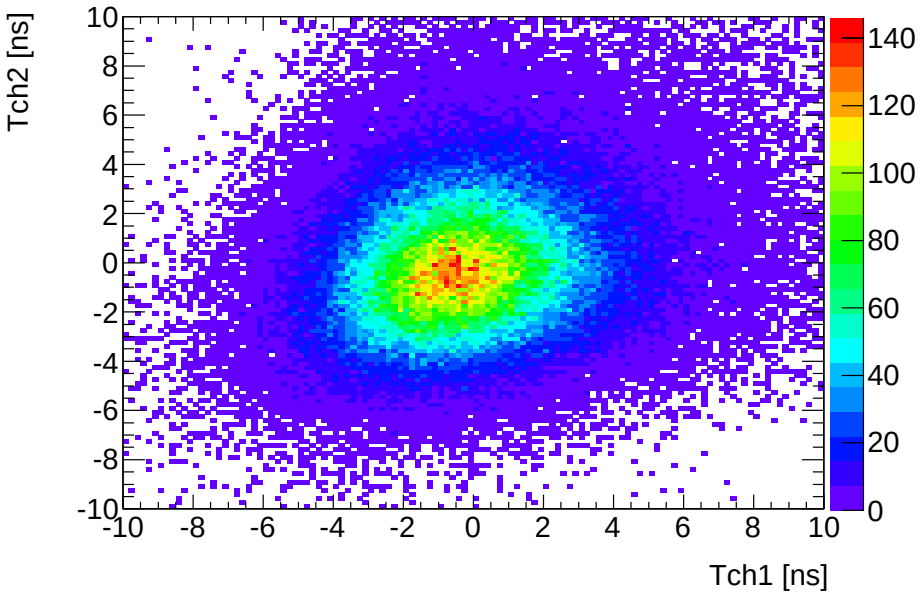

Figure 4.3: The correlation between the time of the channels Tch1 and Tch2

As the occupancy of single particles decreases with increasing energy deposit, the energy interval has been sliced in differently sized bins. Each bin contains at least 200 MeV width and at least 100 events (except the last bin). The sigmas with their errors are plotted as a function of energy, covering mainly the low energy range. The corresponding data decreases at higher energies as expected and it is below 1 ns above 6 GeV. The cell time resolution for high gain is parameterized by the following quadratic sum:

$$\sigma(E) = p_0 \oplus \frac{p_1}{\sqrt{E}} \oplus \frac{p_2}{E} \tag{4.4}$$

where $\oplus$ denotes the square root of the quadratic sum, p_0 is the constant term, p_1 is the stochastic term, p_2 is the noise term and E is the energy deposited in a given cell in GeV. The data, the resolution function and the fit parameters are shown in Figure 4.4.

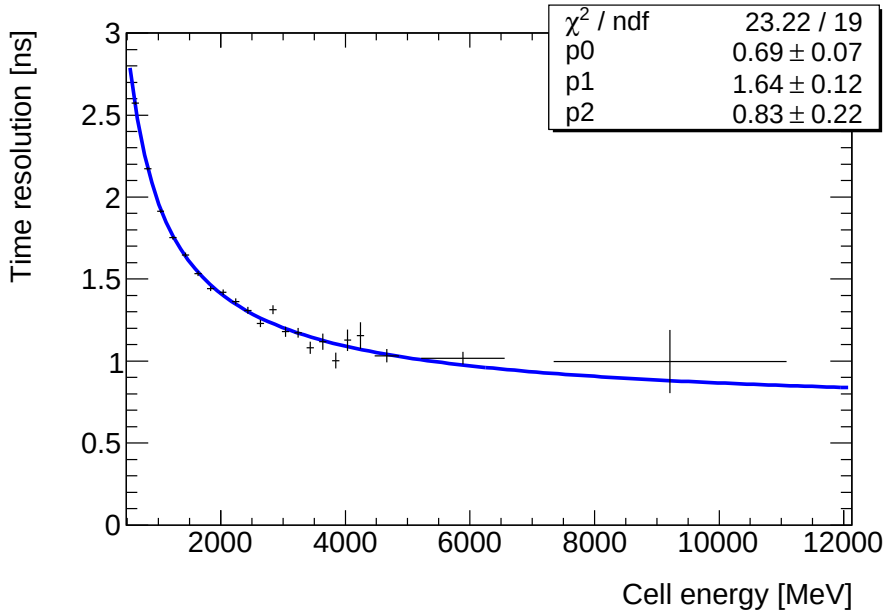

Figure 4.4: Cell time resolution for single hadron collision data

In Figure 4.5, both histogram RMS and Gaussian σ_{T_2} of the cell time distribution are plotted against the energy in logarithmic scale. The tails cause the difference especially at the low energy range.

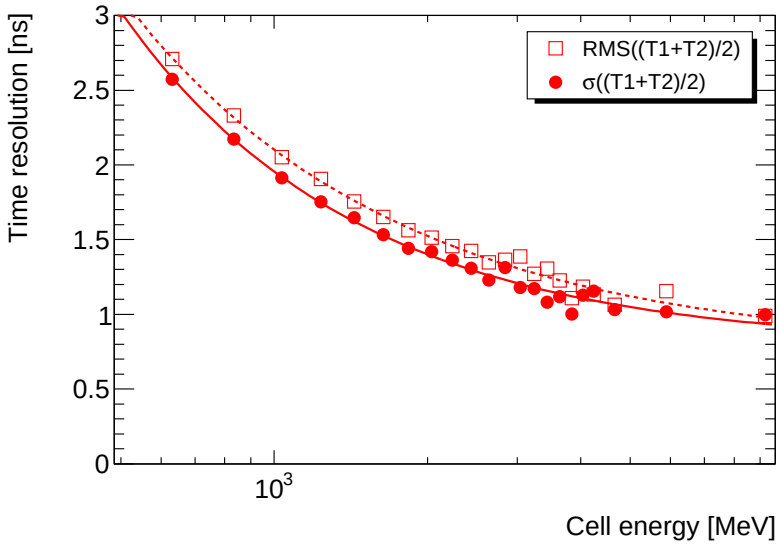

Figure 4.5: Difference between Gaussian sigma and histogram RMS

The timing reconstruction and consequently the resolution is affected by an asymmetric energy deposition in PMT1 (E_1), PMT2 (E_2) by which the cell is readout. Two variables can be considered: $E_{diff} = (E_1 - E_2)/2$ and $E_{cell} = (E_1 + E_2)/2$. The asymmetry is then represented by the following quantity: $\phi' = E_{diff}/E_{cell}$. The dependence of time resolution on ϕ' is plotted in Figure 4.6 (a). The timing performance misbehaves for $\phi' > 0.6$. Since 99% of the statistics is under $\phi' = 0.603$ (see Figure 4.6 (b)), this effect is negligible for overall computations.

In order to improve the cell time resolution, one can synchronize all cells using the single hadron data. The T_2 distributions are plotted for each one of 4416 considered cells and the corresponding mean times are stored. One have to account for $\langle T_2 \rangle$ as a function of energy i.e. determine mean times for each cell in a given interval of energy. However, this analysis is limited by low statistics and the integration over wider range is necessary. Subsequently, the individual cell time spectra are justified and centered at $\langle T_2 \rangle = 0$. Unfortunately, again due to lack of events, it is possible to synchronize only 22% cells. Moreover, the error of estimating the mean value of the distribution is quite high and the cell alignment is thus affected. Figure 4.7 demonstrates the improvement of time resolution after this upgrade. The time resolution is 1 ns at $\sim$ 4.4 GeV. This improvement is notable at higher energy range. An ideal outcome would be achieved if the mean times from jet data were used. The advantage of this collision data is its great

statistics, unlike the single hadron data.

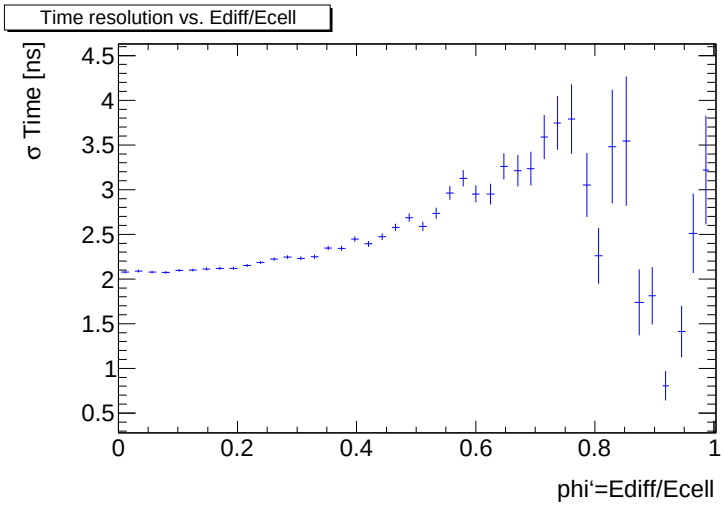

(a) Degradation of the timing performance with increasing ϕ'

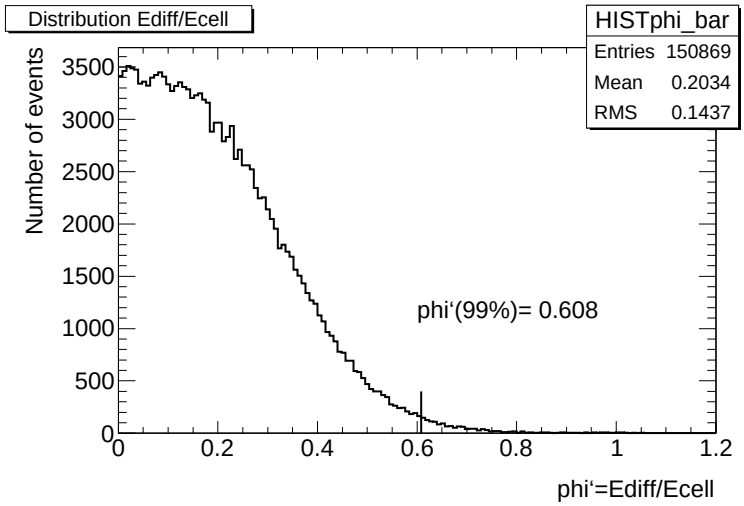

(b) Distribution of ϕ'

Figure 4.6: Asymmetric energy deposition in PMT1 and PMT2

4.2.2 Mean time

The mean time response of single isolated hadrons in the Tile calorimeter also scales with the cell energy. As shown in Figure 4.8, it has decreas-

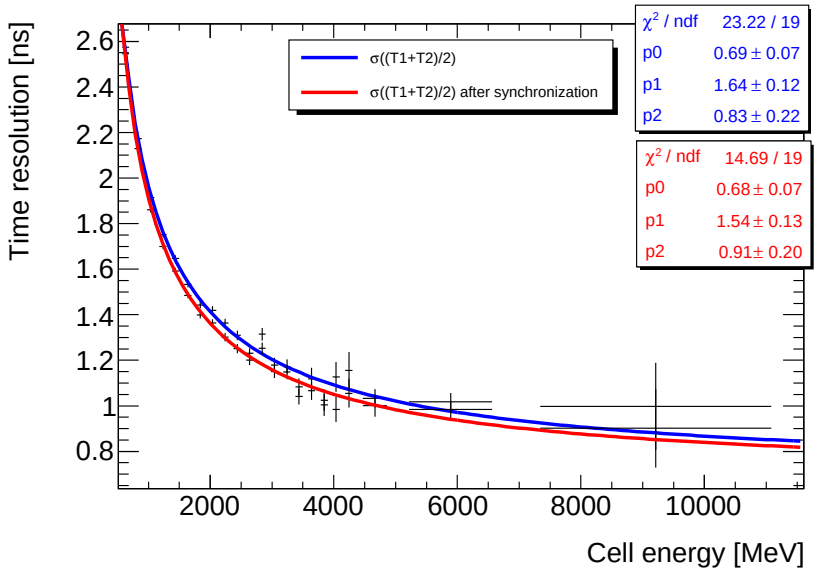

Figure 4.7: Cell time resolution before and after synchronization

ing tendency, probably due to neutron/slow hadronic component of the hadronic showers [22]. Still, this effect is within 1 ns and thus is not so obvious in Figure 4.9 where mean as well as width of cell time distribution are plotted.

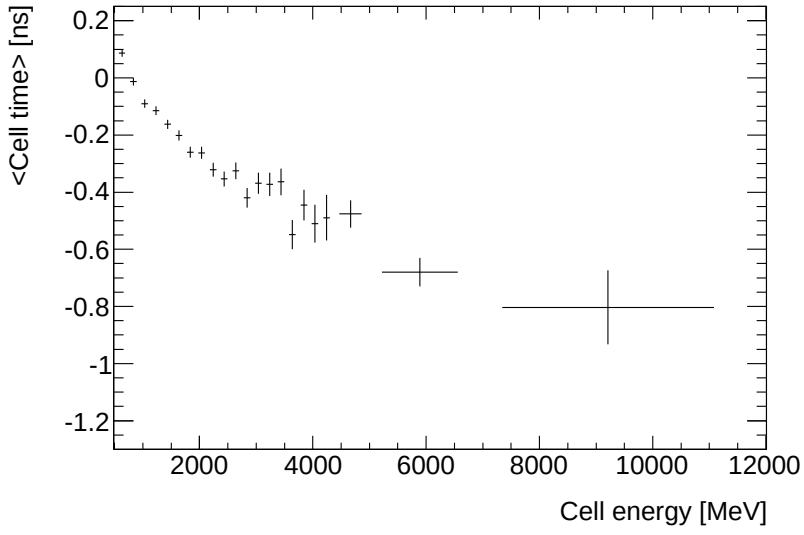

Figure 4.8: Mean cell time

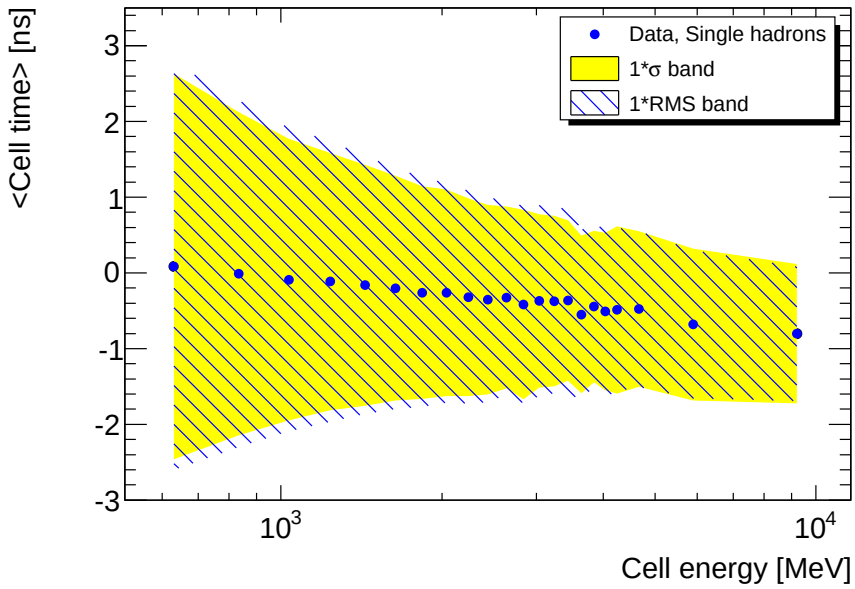

Figure 4.9: Mean and width of the cell time distribution

4.3 Experimental data vs. MC simulation

The results obtained from collision data are compared to Monte Carlo (MC) simulation predictions. The event generation was done with PYTHIA. The phenomenological model to describe *pp* collisions was tuned to reproduce single pion, minimum bias and underlying event data. The ATLAS detector simulation software which is based on GEANT4 [23] has been used to process the generated events. The analysis used for the MC data is the same as that used for the experimental data.

The time resolution for MC data is much better than for real data, as seen in Figure 4.10. This shift is caused by the simplified signal propagation model in TileCal MC. Therefore, some simulation parameters have to be tuned and revised.

The Figure 4.11 compares the mean cell time of both datasets. The energy dependence is accurately described with MC data. However, there is a global offset $\sim$1 ns with respect to the real data. This feature of MC timing is already known and described [24].

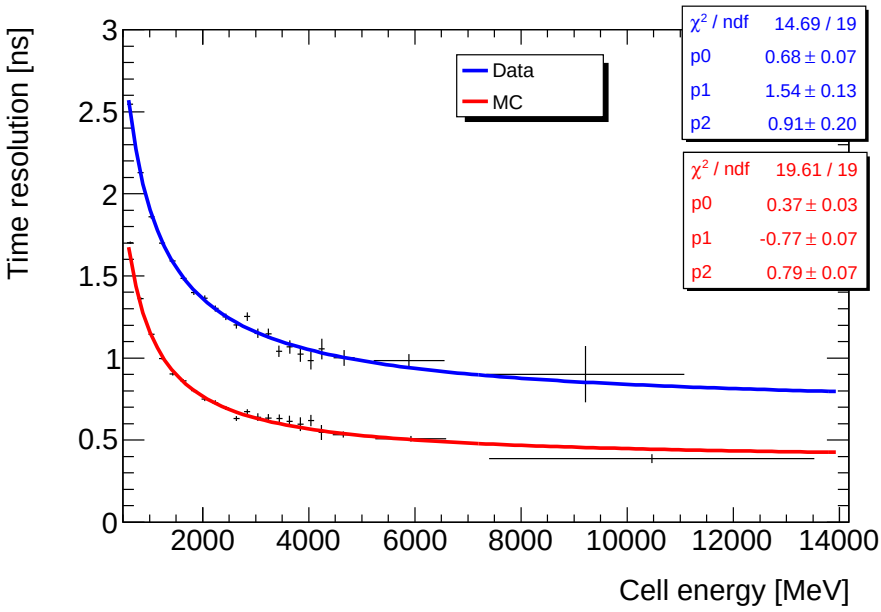

Figure 4.10: Time resolution MC/Data

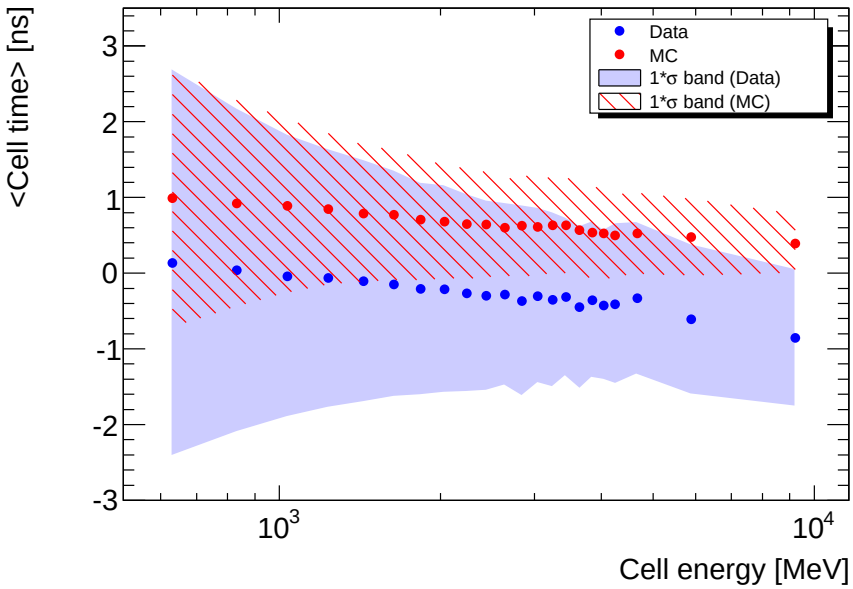

Figure 4.11: Mean time MC/Data

4.4 Comparison with results from jets and muon data

In this section, the results from single hadrons are compared with those from jets and muons obtained by Tomáš Davídek and Javier Montejo.

Cell time resolution as a function of cell energy is shown in Figure 4.12. The time of the cell has been corrected for its mean time. As jets deposit a significant fraction of their energy in TileCal, they uniformly explore the whole energy range under study. Beyond, muons mainly cover the low energy range without reaching the LG region. Since they interact only weakly, the non-Gaussian tails are absent and time distribution shape is perfectly Gaussian. Therefore, the time resolution for muons is better up to 6 GeV. At high energy, its little worsening is caused by low statistics.

Figure 4.13 compares three datasets: jets, muons and single hadrons. The cell time resolution for single pions should be with good agreement with that for jets. In view of limited possibility of time calibration and lack of events, one cannot be surprised by the imperfect correspondence.

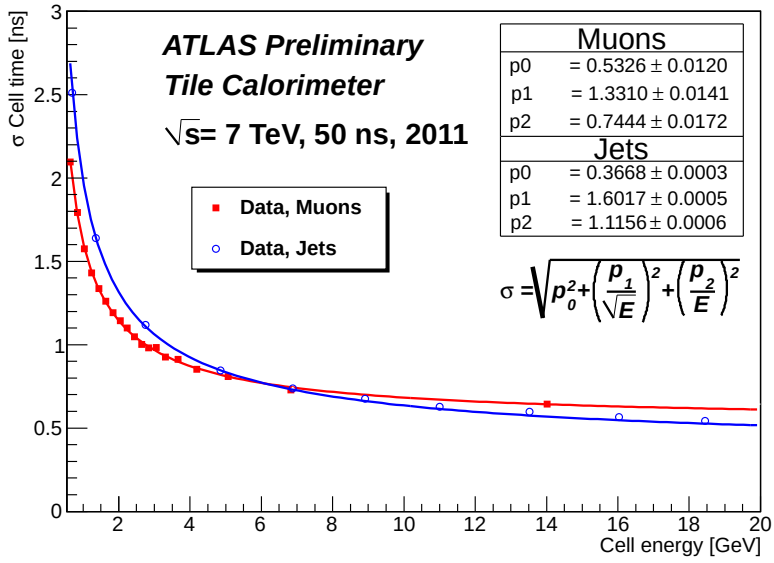

Figure 4.12: Cell time resolution for jets and isolated muons [22]

In Figure 4.14, mean cell reconstructed time as a function of energy deposited in the cell is shown. Left plot is obtained with isolated muons,

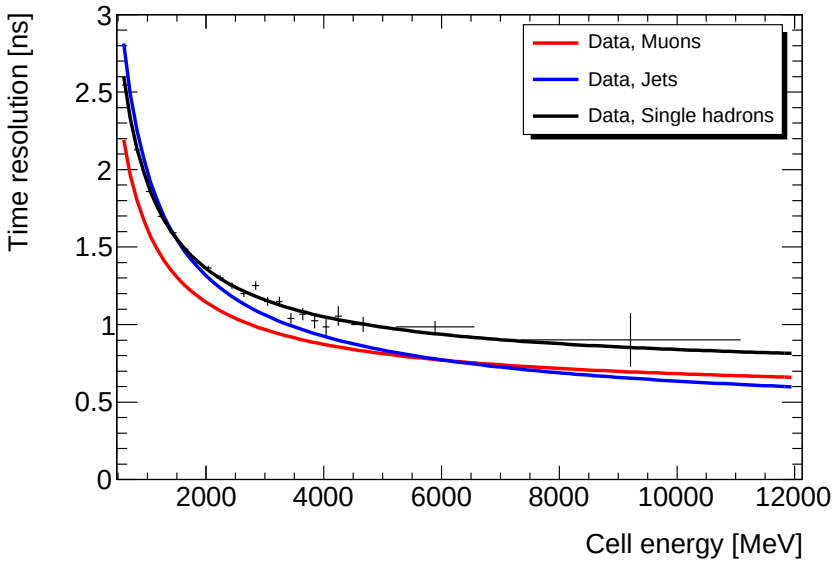

Figure 4.13: Cell time resolution for jets, isolated muon and single hadrons

right plot with jets (p_T >20 GeV). The mean muon time response is very close to zero and essentially independent of the deposited energy as expected [22]. The mean time for jets decreases more sharply than single hadrons likely due to larger slow hadronic component of the hadronic showers.

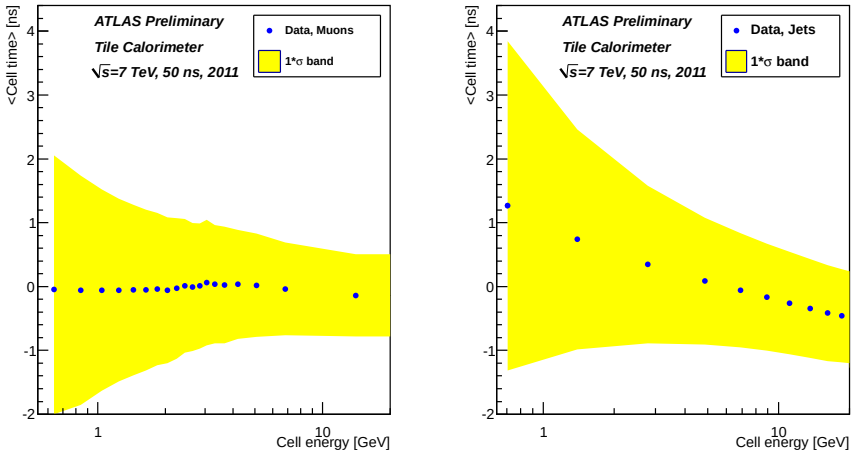

Figure 4.14: Mean time for jets and isolated muons [22]

Chapter 5

Detection of heavy stable particles with Tile Calorimeter

The existence of so far unobserved long-lived massive particles is predicted by a range of theories which extend the Standard Model. This chapter details their expected response in ATLAS and focuses on their search using time-of-flight measurement performed by the Tile Calorimeter.

5.1 Stable Massive Particles

The Standard Model (SM) of the fundamental particles and their interactions is extremely successful theory. Up to now, a lot of experiments at the energy scale of hundreds of GeV have been performed with no confirmed deviation from the SM predictions. However, there are some phenomena that are not explained by the SM, such as the nature of the dark matter, the gravitational interaction and the so-called gauge hierarchy problem. Thus, the SM is not a complete theory and may be a low-energy approximation of a larger theory e.g. the supersymmetry or the universal extra dimensions. The energy of LHC is high enough to probe the physics at the TeV scale. In many extensions of SM, there occur new Stable Massive Particles[7] (SMPs), summarized in [25].

5.1.1 Theoretical motivation

Among the more plausible scenarios of physics beyond the SM is supersymmetry (SUSY). The Minimal Supersymmetric Standard Model (MSSM) is

[7]The term stable means that the particle has a decay length comparable to the size of the ATLAS detector or longer.

the minimal extension to the SM that realizes the supersymmetry. This theory predicts that every elementary particle of SM has sparticle superpatner whose spin differs by a half. Since these particles have not been observed so far, there must exist a mass gap between the SM particles and their superpartners, implying that supersymmetry must be broken. This opens the possibility that the supersymmetry eigenstates do not correspond to the mass eigenstates, and therefore the possibility of mixing between sparticle states with the same quantum numbers. As a result, the photino ($\tilde{\gamma}$), zino ($\tilde{Z}$), and neutral Higgsinos ($\tilde{H}^0_{1,2}$) mix to form four neutralinos $\tilde{\chi}^0_{1,2,3,4}$, where $\tilde{\chi}^0_1$ stands for the lowest-mass linear superposition. The wino ($\tilde{W}^{\pm}$) and charged Higgsinos ($\tilde{H}^{\pm}_{1,2}$) mix to form two charginos $\tilde{\chi}^{\pm}_{1,2}$.

The superpotential of the most general SUSY models includes the terms which violate both lepton and baryon number [26]. It can lead to rapid proton decay and thus can make the models phenomenologically invalid. For these reasons, the conservation of the quantum number $R = (-1)^{3B+L+2S}$ is postulated [25], where B/L is baryon/lepton number and S is spin of a particle. This R-parity distinguishes a particle ($R = +1$) from its superpartner ($R = -1$) ensuring that the supersymmetric partners of SM states can only be pair produced. Moreover, the lightest supersymmetric particle (LSP) cannot decay in to a pair of SM particles and remains stable, providing a possible solution to the dark-matter problem.

The search for SMPs is usually performed in the framework of two SUSY models, gauge mediated SUSY breaking (GMSB) and split SUSY described below.

Gauge Mediated SUSY Breaking

In this model, the supersymmetry is broken by gauge interactions involving messengers between the visible and the hidden sector. GMSB allows for the gravity. The gravitino $\tilde{G}$ (the supersymmetric partner of the graviton G) is very light ($m_{\tilde{G}} < 1$ keV) and hence the LSP [25]. The next-to-lightest sparticle (NLSP) decays only via the gravitational coupling and can be very long-lived. The **slepton** ($\tilde{l}$) play the role of charged NLSP with long lifetime i.e. SMP. However, in the case of the small lifetime, the distinguishing feature of its decay to the gravitino $\tilde{l} \to l\tilde{G}$ would be event with energetic lepton and significant missing energy due to the missing gravitino [28].

Split SUSY

In the so-called split SUSY scenario, the masses of the supersymmetric fermions (gaugino and higgsino) are assumed to be at the TeV range while all the scalars (sleptons and squarks), apart from a Higgs boson, are at the very high mass scale. Therefore, gluinos $\tilde{g}$ can be accessible by the ATLAS experiment in pp collisions at LHC. Feynman diagrams for their production at hadron collider are plotted in Figures 5.1 and 5.2. Since the colored gluinos can only decay via heavy squarks, their lifetime can be very large and they hadronize into heavy (charged or neutral) bound states, called ***R*-hadrons**. An R-hadron can be a R-meson ($\tilde{g}q\bar{q}$), a R-baryon ($\tilde{g}qqq$) or a "glueball" ($\tilde{g}g$). In this model, the R-hadrons represent the SMPs and the neutralinos $\tilde{\chi}_1^0$ are the LSPs.

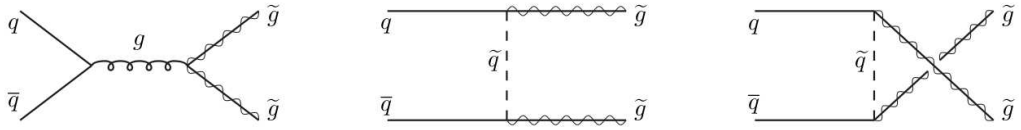

Figure 5.1: Feynman diagrams for gluino production at hadron collider from strong quark-antiquark annihilation [27].

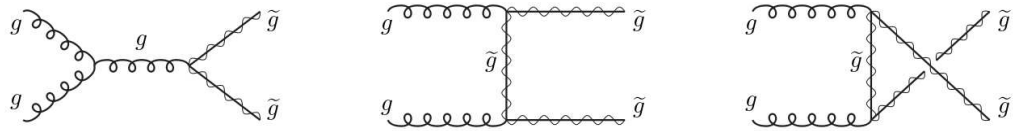

Figure 5.2: Feynman diagrams for gluino production at hadron collider from gluon-gluon fusion [27].

5.1.2 Expected detector response in ATLAS

The SMPs produced at LHC energies typically have the following model-independent features: they are usually penetrating[8] and travel with velocity significantly lower than the speed of light $\beta \ll 1$.

[8] A small fraction of SMPs can be brought to rest by interactions in the detector. Subsequently, an alternative approach to their direct detection would be to observe their decays, see Ref. [29].

Long lived slepton interaction

The long-lived slepton would interact like heavy muons leaving signals throughout all the detector from the ID to the MS including the calorimeters. Being a slow-moving charged particle, its ionization energy deposit is anomalously high and its bremsstrahlung radiation is reduced. Therefore, no electromagnetic shower is developed. In addition, since it is a color-singlet, it is not expected to produce hadronic shower.

Long lived R-hadron interaction

The charge R-hadron can lose its energy through nuclear interactions and ionization losses, the neutral one only through the former. The probability that the heavy supersymmetric parton will interact perturbatively with the quarks in the target nucleon is small, since such interactions are suppressed by a factor $1/m^2$ where m is the mass of parton [30]. As a consequence, only the light quark system (LQS) is responsible for the interactions and the heavy parton acts as spectator. Moreover, LQS carries very small fraction of the kinetic energy of the hadron, meaning that the effective interaction energy of the hadron is very low. In these low-energetic scattering processes, exchange of electric charge and baryon number can occur. All R-hadron processes can be derived by exchanging quarks, as seen in Table 5.1. It should be noted that the R-meson processes with baryon exchange are kinematically favored, unlike the R-baryon processes. Therefore, mesons get converted into baryons during repeated interactions, but not vice versa.

	R-meson	R-baryon
Elastic scattering	$\tilde{g}d\bar{d} + uud \to \tilde{g}d\bar{d} + uud$	$\tilde{g}uud + uud \to \tilde{g}uud + uud$
Charge exchange	$\tilde{g}d\bar{d} + uud \to \tilde{g}u\bar{d} + udd$	$\tilde{g}uud + udd \to \tilde{g}udd + uud$
Baryon exchange	$\tilde{g}d\bar{d} + uud \to \tilde{g}udd + u\bar{d}$	–

Table 5.1: Gluino R-hadrons in $2 \to 2$ processes

5.1.3 Search for SMPs with ATLAS

The SMPs can be identified and their mass M determined by measurement of momentum p and velocity β using the following relation:

$$M = \frac{p}{\beta\gamma} \tag{5.1}$$

Two different searches are presented, the first one is based on the muon spectrometer (MS) measurement and the second one requires only signals in the ATLAS inner detector (ID) and calorimeters.

Muon spectrometer-based search

In this method, only the particles arriving as charged to the muon spectrometer are considered candidates. The limit $\beta > 0.5$ is required for a correct reconstruction of the track in muon system [31]. The MS signals left by an SMP with lower speed may be associated with the next bunch crossing and lost during data taking. The velocity is measured using timing information from the muon system, and Tile Calorimeter when available. The *slepton search* employs a combined reconstruction method which requires combined ID and MS tracks. The momentum is then obtained from the combined track. The *charged R-hadron search* is based on a MS-standalone reconstruction method i.e. does not require a track in ID. Accordingly, the momentum is measured from the standalone track. However, in case of the charged heavy hadron without charge-flipping in the calorimetry, an ID track can be associated with the standalone candidate and combined.

This MS based search for SMPs has been widely studied and performed, see Ref. [32]. No excess was observed above the estimated background and limits on SMP production were set. Stable staus $\tilde{\tau}$ are excluded up to a mass of 136 GeV and sleptons produced in electroweak processes are excluded up to a mass of 110 GeV. Gluino R-hadrons in the scattering model of Ref. [30] are excluded up to masses of 530 GeV to 544 GeV depending on the fraction of R-hadrons produced as $\tilde{g}g$ states.

Muon spectrometer-agnostic search

This method does not require any signals in the MS and the momentum measurement relies in having a charged particle that produces a signal in the ID tracking systems. Two complementary subsystems are used to distinguish SMPs from particles moving at velocities close to the speed of light and to measure their velocity β: the Pixel detector and the TileCal.

The *Pixel detector* offers detailed measurements of the deposited energy per unit length dE/dx. The mean energy loss is given by the Bethe-Bloch formula and to a good approximation depends only on the speed of the particle β. However, the full equation is not analytically invertible. For values of dE/dx considerably larger than the expected value for a MIP (minimum ionizing particle), the stopping power is dominated by a $1/\beta^2$

and thus invertible. This is exactly the case of high-mass signal scenarios such as the SMPs. Moreover, by plotting the expected specific energy loss as a function of momentum p, the curves are shifted for different masses. The shift provides the separation between the SM particles and the SMPs, see Figure 5.3.

The *TileCal* measures the Time-of-Flight (ToF) for particles which traverse it. The heavy long-lived particles are expected to have such a high mass that they can be regarded as nonrelativistic. Unlike the SM particles, their detector response is delayed and consequently can be used for their detection. The speed β of an SMP candidate is then determined using the time measurement of the TileCal cell in which it deposited its energy. This technique is covered in more detail in Section 5.2.

In this ATLAS search for SMPs [33], the observed limits are 562 to 586 GeV for gluino R-hadrons. The range comes from varying the hadronic scattering model and the spectrum of possible R-hadron states.

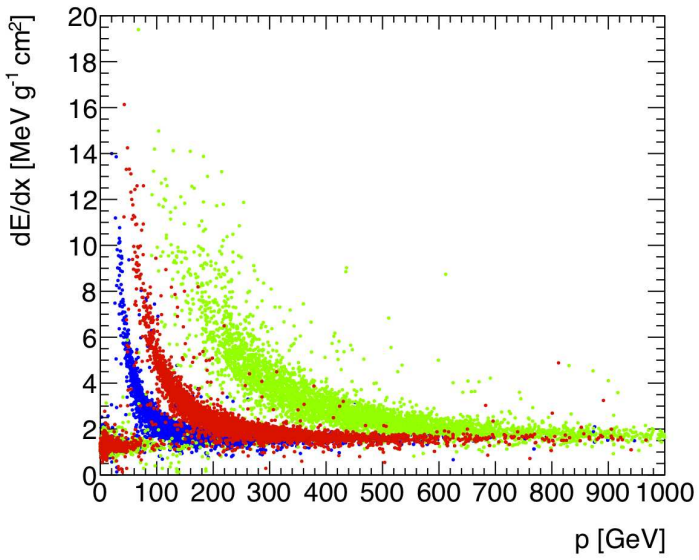

Figure 5.3: The expected specific energy loss as a function of momentum for tracks in simulated events with gluino R-hadrons of mass 100 GeV (blue), 200 GeV (red) and 500 GeV (green). Since the resolution of the momentum degrades with momentum, the bands grow thicker with mass. The band at lower momenta around the MIP value corresponds to SM particles [34].

To sum up, the search for SMPs depends on their type and their response in ATLAS. There are following possibilities to identify them and determine their mass:

- Charged exotic particles, such as sleptons and charged R-hadrons, with velocity $\beta > 0.5$ leave the signal in all subdetectors. This signature allows to combine both methods in order to improve the mass resolution.
- Charged R-hadrons can be converted to neutral within the dense calorimeter. In this case, only the muon spectrometer-agnostic search is available.
- Initially neutral R-hadrons interact hadronically and can thus undergo charge-flipping. If these charged R-hadrons cross the muon spectrometer with the speed $\beta > 0.5$, the MS measurements can be improved using ToF measurement performed by the TileCal.
- Neutral R-hadrons have no track either in the inner detector or in the muon spectrometer. Therefore, only the TileCal ToF measurement can identify these particles. However, the possibility to accurately reconstruct their mass is limited.

5.2 Search using Time-of-Flight technique in Tile Calorimeter

As shown in the previous chapter, the hadronic Tile calorimeter offers great time resolution and enables precise time-of-flight measurement for particles traversing it. In this section, the discovery potential of SMPs using the TileCal time measurement is discussed.

A calorimeter-based measurement has two main benefits. Firstly, the event fragments from different subdetectors are assigned to a particular bunch crossing (BC) using the BC identifier (BCID). Each detector is calibrated with respect to the particles which move practically at the speed of light $\beta \approx 1$ and thus the slow SMPs may be marked with a wrong BCID and lost during data taking. Since the calorimeter is placed more closely to the interaction point than MS, there is less read-out window problem for slower particles $\beta \ll 1$. Secondly, the great advantage of this method is the detection of the charged as well as the neutral SMPs. In the case of neutral hadronically interacting particles, the possibility to accurately reconstruct their mass is limited because of the absence of their tracks in ID and MS. However, they can undergo charge exchange when passing through the dense calorimeters and their signature can thus have a track in MS. On the other hand, if the particles are initially charged and convert to the neutral ones, the track in MS is absent.

Each TileCal cell provides the time measurement t_{ToF}. In this analysis, only cells with a measured energy deposition greater than 540 MeV are considered. The velocity β_i of a particle that deposits energy in a cell i located at a distance $L_{cell,i}$ from the interaction point can be estimated as follows:

$$\beta_i = \frac{v_{cell,i}}{c} = \frac{L_{cell,i}}{t_{ToF,i}c} = \frac{L_{cell,i}}{(t_{reco,i} + t_{cell,i})c} \tag{5.2}$$

where $t_{reco,i}$ is the reconstructed cell time and $t_{cell,i}$ is the time-of-flight of the relativistic particle to a cell i. The latter is a constant determined for each cell.

Since SMPs are mostly penetrating, they tend to traverse the entire TileCal, leaving statistically independent signals in up to six cells. Therefore, the corresponding β_i values can be combined to increase the precision for a given track. In the previous chapter, there was demonstrated that the cell time resolution improves at larger energy depositions. Therefore, the velocity $\bar{\beta}$ is calculated as a weighted average:

$$\bar{\beta} = \frac{\sum_{i=1}^{n} w_i \beta_i}{\sum_{i=1}^{n} w_i} \tag{5.3}$$

where n is the number of cells along the path where the energy deposited has exceeded a given threshold and w_i is the weight for the measurement of β_i and is a function of the measured energy, $w_i \equiv w(E_i) = E_i$.

When the particle's momentum p (ID) and velocity β (TileCal) are measured, its mass could be determined by the following equation:

$$M(p, \bar{\beta}) = p\frac{\sqrt{1 - \bar{\beta}^2}}{\bar{\beta}} \tag{5.4}$$

Accordingly, the mass resolution is then given by:

$$\sigma_M(p, \bar{\beta}) = \frac{\partial M(p, \bar{\beta})}{\partial p}\sigma_p \oplus \frac{\partial M(p, \bar{\beta})}{\partial \bar{\beta}}\sigma_{\bar{\beta}} \tag{5.5}$$

where σ_p is the approximate precision of momentum measurement with ID [20] and $\sigma_{\bar{\beta}}$ is the precision of velocity measurement with TileCal. The latter is connected to the time resolution $\sigma_{t_{reco}}$, which was evaluated in the previous chapter, through the Equations 5.2 and 5.3. Their values are the following:

$$\sigma_p(p) = 3.6 \cdot 10^{-4}\ p^2 \oplus 3.6 \cdot 10^{-2} \tag{5.6}$$

$$\sigma_{t_{reco}}(E) = 0.68 \oplus \frac{1.54}{\sqrt{E}} \oplus \frac{0.91}{E} \tag{5.7}$$

where p and E are in GeV.

To evaluate the time resolution of the TileCal, the assumptions about the energy loss of the heavy exotic particles have been made:

The ionization losses in the TileCal have been parameterized as $E_{ioniz} = K/\beta^2$. The constant K is a measured value of the most probable muon losses in the calorimeter at small pseudorapidities and is equal to 2.2 GeV [20].

The energy loss due to purely nuclear interactions of an R–hadron have been widely studied in [30]. According to a proposed model describing nuclear interactions of heavy hadrons, the interaction length in iron of an R-baryon[9] is 14 cm. Since the thickness of the Tile calorimeter at $\eta \sim 0$ is 1.52 m corresponding to 1.2 m of iron, the average number of nuclear interactions is 9. The amount of energy lost in a collision in iron for the mass $M = 600$ GeV can be estimated from the Figure 5.4. Altogether, hadronic losses of R-hadrons with mass $M = 600$ GeV in TileCal are roughly equal to 1.5% of their kinetic energy.

To get an estimate of the mass resolution of an SMP, one can assume that the particle traverses the TileCal at $\eta \sim 0$ leaving the signal in cells A1, BC1 and D0. Their positions and dimensions are introduced in the Table 5.2.

Cells	R [mm]	DR [mm]	t_0 [ns]
A1	2450	300	8.2
BC1	3020	840	10.1
D0	3630	380	12.1

Table 5.2: The positions and dimensions of the cells A1, BC1 and D0. R stands for the radial position of the cell center, DR represents radial dimension of the cell and t_0 is the ToF of relativistic particles for the individual cell.

[9] After traveling 20 cm in iron, 50% of R-mesons are converted into R-baryons.

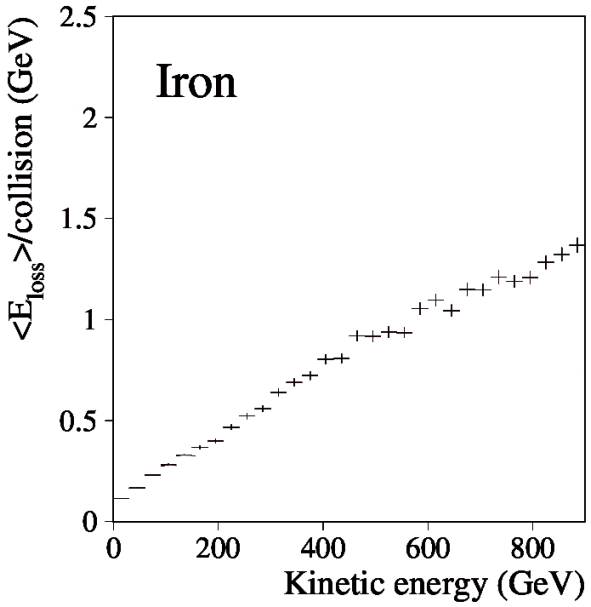

Figure 5.4: The mean value of the average energy loss per collision of an R–baryon with mass $M = 600$ GeV [30].

Subsequently, the combined speed measurement $\bar{\beta}$ is calculated as follows:

$$\bar{\beta} = \frac{E_1\beta_1 + E_2\beta_2 + E_3\beta_3}{E} \tag{5.8}$$

where E_1, E_2 and E_3 stand for the total energy losses i.e. the sum of nuclear energy losses and ionization losses in cells A1, BC1 and D0, respectively. The sum of energy deposited in all three cells is represented by E.

The mass resolution of an SMP resulted from Equation 5.5 is then:

$$\frac{\sigma_M}{M} = \frac{\sigma_p}{p} \oplus \frac{\beta_1^2}{\bar{\beta}(1-\bar{\beta}^2)} \frac{E_1}{E} \frac{\sigma_{t_{reco1}}}{t_{01}} \oplus \frac{\beta_2^2}{\bar{\beta}(1-\bar{\beta}^2)} \frac{E_2}{E} \frac{\sigma_{t_{reco2}}}{t_{02}} \oplus \frac{\beta_3^2}{\bar{\beta}(1-\bar{\beta}^2)} \frac{E_3}{E} \frac{\sigma_{t_{reco3}}}{t_{03}} \tag{5.9}$$

where $\sigma_{t_{reco1}} \equiv \sigma_{t_{reco1}}(E_1)$ i.e. the time resolution of the cell A1 depends on the energy deposited in this cell E_1. The same holds for all cells. After putting $\bar{\beta} = \beta_1 = \beta_2 = \beta_3 = p/\sqrt{p^2 + M^2}$, one can write:

$$\frac{\sigma_M}{M} = \sqrt{\frac{\sigma_p^2}{p^2} + \frac{p^2(p^2+M^2)}{M^4}\frac{1}{E^2}\left(\left(E_1\frac{\sigma_{t_{reco1}}}{8.2}\right)^2 + \left(E_2\frac{\sigma_{t_{reco2}}}{10.1}\right)^2 + \left(E_3\frac{\sigma_{t_{reco3}}}{12.1}\right)^2\right)} \tag{5.10}$$

Here, it would be appropriate to mention also the mass resolution derived from the velocity measured only by the closest to the ATLAS interaction point TileCal cell A1:

$$\frac{\sigma_M}{M} = \sqrt{\frac{\sigma_p^2}{p^2} + \frac{p^2(p^2+M^2)}{M^4}\left(\frac{\sigma_{t_{reco1}}}{8.2}\right)^2} \tag{5.11}$$

The energy loss of an SMP in TileCal and hence the time resolution depends on its type. As the signal in the ID tracking signal is required in order to identify the particle and determine its mass using the ToF discovery method, it has to be initially charged. There are three possibilities that have to be considered individually. Firstly, a charged R-hadron loses energy through the electromagnetic as well as the nuclear interactions. Secondly, an R-hadron can undergo charge exchange when passing through the calorimeters and become neutral in TileCal. Consequently, it deposits the energy only through the hadronic scattering processes. Thirdly, slepton suffers purely the continuous ionization losses. Table 5.3 summarizes the energy depositions of each SMP type for a cell A1.

Charged R-hadrons	$E_1 = E_{ioniz1} + E_{hadr1}$
Neutral R-hadrons	$E_1 = E_{hadr1}$
Sleptons	$E_1 = E_{ioniz1}$

Table 5.3: The energy losses of charged R-hadrons, neutral R-hadrons and sleptons in TileCal.

Thereafter, the ionization losses E_{ioniz} and the nuclear energy losses E_{hadr} for an SMP with mass $M = 600$ GeV in a cell A1 can be written as follows [20, 30] :

$$\begin{aligned} E_{ioniz1} &= 0.2 \cdot \tfrac{2.2}{\beta_1^2} = 0.2 \cdot 2.2 \cdot \tfrac{p^2+M^2}{p^2} && \text{[GeV]} \\ E_{hadr1} &= 0.2 \cdot 0.015 \cdot T_1 = 0.2 \cdot 0.015 \cdot (\sqrt{p^2+M^2} - M) && \text{[GeV]} \end{aligned} \tag{5.12}$$

where the number 0.2 results from DR_1/DR_{All} (see Table 5.2) and therefore represents the fraction of the traversed path in the cell A1.

Finally, the mass resolution σ_M/M for an exotic heavy stable particle with mass $M = 600$ GeV which leaves the signal in a cell A1 is plotted as a function of its momentum p in a Figure 5.5. To ensure that the signal in this cell is seen within a correct bunch crossing, a limit of a range of ToF measurement has to be taken account. For a bunch crossing of 25 ns, this means that the minimum β is given by: $\beta > 8.2\text{ns}/(8.2 + 25)\text{ns} = 0.25$ and the corresponding limit of a momentum is: $p > 155$ GeV. As the present bunch spacing is 50 ns, a possible range can be extended: $\beta > 8.2\text{ns}/(8.2+50)\text{ns} = 0.14$ and $p > 85$ GeV. Furthermore, since the energy deposition in a cell has to be greater than 540 MeV, the following conditions for ionization loss and nuclear energy loss are applied: $p < 1260$ GeV and $p > 500$ GeV, respectively. The former is out of the range and the latter is indicated in the plot by a dotted line. As expected, the behavior of a function representing only the ionization losses differs from that corresponding to the hadronic losses. This feature is caused by the contribution of the time resolution to the total uncertainty of the mass measurement.

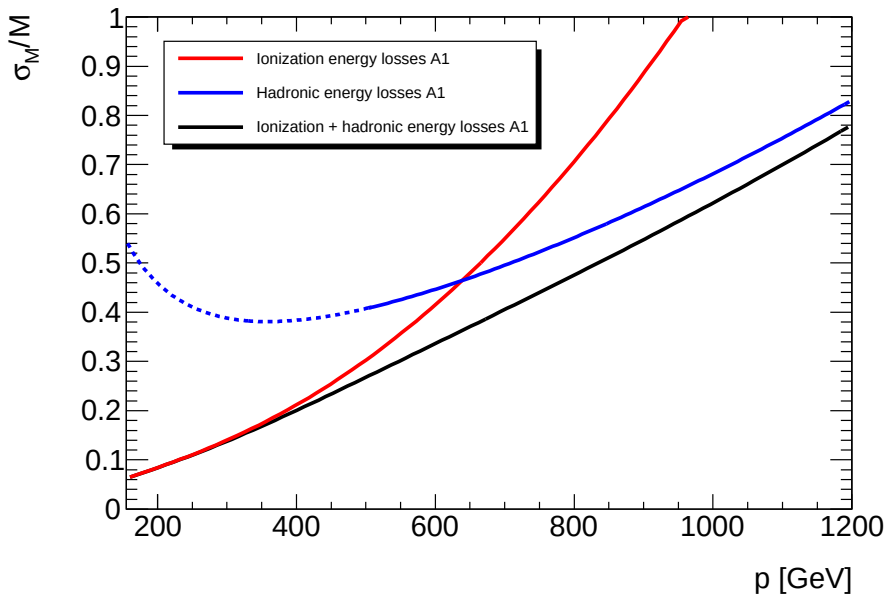

Figure 5.5: Mass resolution σ_M/M for an SMP with mass $M = 600$ GeV as a function of its momentum. Red, blue and black lines correspond to only ionization energy losses, purely hadronic and ionization plus hadronic energy losses of the particle in a cell A1, respectively.

Figure 5.6 shows the mass resolution improvement after combining three independent measurements in cells A1, BC1 and D0. This comparison of single and combined velocity measurement is made for a charged R-hadron with mass $M = 600$ GeV that loses energy through the electromagnetic and nuclear interactions. Since the cell D0 is farther from the interaction point, a possible range od measurement is reduced: $\beta > 12.1\text{ns}/(12.1+25)\text{ns} = 0.33$ and $\beta > 12.1\text{ns}/(12.1+50)\text{ns} = 0.20$ for bunch crossings of 25 ns and 50 ns, respectively. The corresponding momentum limits are then: $p > 210$ GeV and $p > 122$ GeV. The former is reflected in a plot by a dotted line.

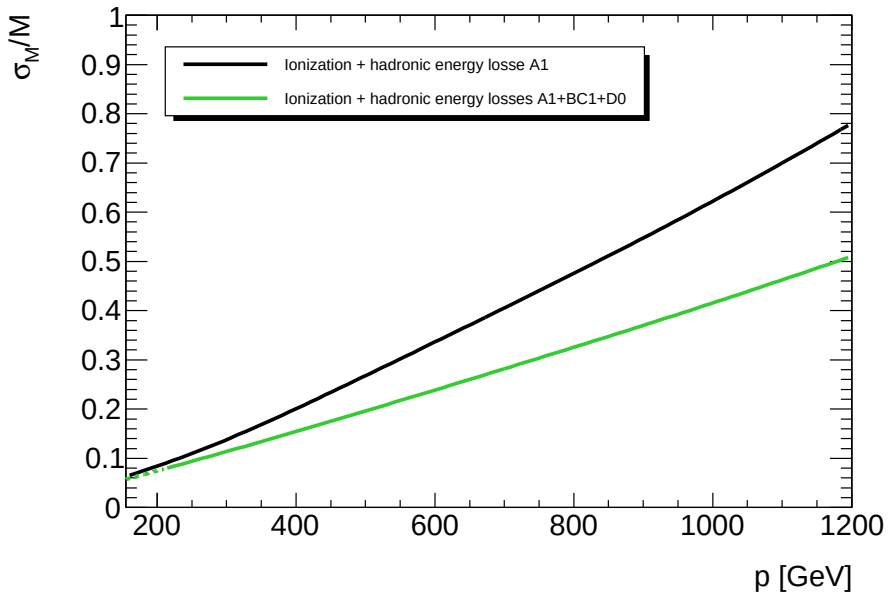

Figure 5.6: Mass resolution σ_M/M for an charged R-hadron with mass $M = 600$ GeV as a function of its momentum. Black line corresponds to the single cell (A1) measurement and the green line represents the combined (A1+BC1+D0) measurement.

Chapter 6

Summary and conclusion

Hitherto unobserved heavy particles stable enough to be detected prior to their decay [32, 33, 34] are predicted by a range of theories which extend the Standard Model. As they propose solution to the gauge hierarchy problem, their discovery would be of fundamental significance.

In this thesis, the discovery potential of the ATLAS detector for the stable massive particles was discussed. Special emphasis was placed on the search using time-of-flight technique in Tile Calorimeter. Therefore, the TileCal timing analysis using the single isolated hadron collision data was performed.

The results from collision data proved that the hadronic calorimeter offers great time resolution and enables precise time-of-flight measurement for particles traversing it. Namely, the cell time resolution that, as expected, depends on the energy deposited in a given cell is better than 1 ns above 4.4 GeV. Moreover, it has been shown that the mean time response of single hadrons also scales with the cell energy. Its subtle decrease within 1 ns is caused by the slow hadronic component of the hadronic shower.

The comparison with the Monte Carlo simulation predictions reveals the global offset in the time resolution as well as in the mean cell time. This shift is caused by the simplified signal propagation model in TileCal simulation. However, the energy dependence is described accurately with MC data.

Besides, the outcomes were compared to the previous analysis with jets and collision muons. At high energy, the cell time resolution of the single hadrons is worse than that of other datasets. This is caused by the low statistics and limited possibility of time calibration.

Finally, the mass resolution of an SMP with mass $M = 600$ GeV using TileCal time-of-flight measurement was estimated. It has been assumed that it traverses the TileCal at $\eta \sim 0$ and leaves the signal in cells A1,

BC1 and D0. The appropriate plot has shown that the mass resolution depends on the processes through which the particle loses its energy i.e. on the type of SMP. Furthermore, the mass is determined more precisely after combining three independent measurements in cells A1, BC1 and D0.

The results obtained in this analysis indicate a strong ability of ATLAS to measure heavy long-lived exotic particles with electromagnetic and/or hadronic interactions.

Bibliography

[1] ATLAS collaboration: *The ATLAS Experiment at the CERN Large Hadron Collider*, JINST 3 S08003, 2008

[2] ATLAS collaboration: *Readiness of the ATLAS Tile Calorimeter for LHC collisions*, Eur. Phys. J. C (2010) 70: 1193–1236

[3] Amaral P. et al.: *Hadronic shower development in Iron-Scintillator Tile Calorimetry*, Nuclear Instruments and Methods in Physics Research A 443 (2000) 51-70

[4] Torres J. P.: *Energy Reconstruction in the Hadronic Tile Calorimeter and Early SUSY Fully Hadronic Searches in ATLAS*, CERN-THESIS-2008-094

[5] Anderson K. et al.: *At the leading edge: the ATLAS and CMS LHC experiments*, World Scientific, 2009

[6] Nordkvist B.: *Time Calibration of the ATLAS Tile Calorimeter using an Integrated Laser System*, Journal of Physics: Conference Series 219 (2010) 022015

[7] Anderson K. et al.: *ATLAS Tile Calorimeter Interface Card*, Proc. of the 8th Workshop on Electronics for LHC Experiments, ISBN 92-9083-202-9 (2002)

[8] Christiansen J., Marchioro A., Moreira P., Toifl T.: *TTCrx Reference Manual: A Timing, Trigger and Control Receiver ASIC for LHC Detectors*, http://ttc.web.cern.ch/TTC/TTCrx_manual3.9.pdf

[9] Bohm C. et al.: *ATLAS Tilecal Digitizer Test System and Quality Control*, CERN-ATL-COM-TILECAL-2004-008, CERN, Geneva, 2004

[10] Davidek T. et al.: *Testbeam studies of production modules of the ATLAS Tile Calorimeter*, Nuclear Instruments and Methods in Physics Research A 606 (2009) 362–394

[11] Usai G.: *Signal Reconstruction of the ATLAS Hadronic Tile Calorimeter: implementation and performance*, Journal of Physics: Conference Series 293 (2011) 012056

[12] Salvachua B. et al.: *Algorithms for the ROD DSP of the ATLAS Hadronic Tile Calorimeter*, JINST 2 T02001, 2007

[13] Valero A.: *Implementation and performance of the signal reconstruction in the ATLAS Hadronic Tile Calorimeter*, ATL-TILECAL-PROC-2011-008

[14] Solans C.: *Performance of the ATLAS Hadronic Tile Calorimeter at the LHC Startup*, ATL-TILECAL-PROC-2009-003

[15] Febbraro R.: *Calibration and signal reconstruction in the ATLAS Tile Hadronic calorimeter*, ATL-TILECAL-PROC-2010-006

[16] Giangiobbe V.: *The TileCal Laser calibration system*, ATL-TILECAL-PROC-2011-007

[17] The ATLAS collaboration: *Response of the ATLAS calorimeters to single isolated hadrons produced in proton proton collisions at a center of mass energy of* $\sqrt{s}$ *= 900 GeV*, ATLAS-CONF-2010-017

[18] The ATLAS collaboration: *ATLAS Calorimeter Response to Single Isolated Hadrons and Estimation of the Calorimeter Jet Scale Uncertainty*, ATLAS-CONF-2011-028

[19] Lampl W. et al.: *Calorimeter Clustering Algorithms: Description and Performance*, ATL-LARG-PUB-2008-002

[20] Leitner R., Shmakova V. V., Tas P.: *Time resolution of the ATLAS Tile calorimeter and its performance for a measurement of heavy stable particles*, ATL-TILECAL-PUB-2007-002

[21] Presentation of J. Montejo:
`https://indico.cern.ch/conferenceDisplay.py?confId=125259`

[22] Davidek T., Montejo J.: *Cell time resolution as a function of cell energy in the collision data at* $\sqrt{s} = 7$ *TeV*, ATLAS-PLOT-TILECAL-2011-012

[23] Agostinelli S. et al.: *G4–a simulation toolkit*, Nucl. Instr. and Meth. A 506 (2003) no. 3, 250 – 303

[24] https://twiki.cern.ch/twiki/bin/view/AtlasPublic/TileCaloPublicResults#Timing

[25] Fairbairn M., Kraan A. C., Milstead D. A., Sjöstrand T., Skands P., Sloan T.: *Stable Massive Particles at Colliders* , CERN, Geneva, December 2006

[26] Vempati S. K.: *Introduction to the MSSM*, Indian Institute of Science, Bangalore, January 2012, arXiv:1201.0334v1

[27] Martin S. P.: *A Supersymmetry Primer*, Fermi National Accelerator Laboratory, Illinois, June 2006, hep-ph/9709356

[28] The OPAL Collaboration.: *Searches for Prompt Light Gravitino Signatures in e^+e^- Collisions at $\sqrt{s}$ =189 GeV*, CERN-EP-2000-078, May 2000

[29] The CMS Collaboration: *Search for Stopped Gluinos in pp collisions at $\sqrt{s}$ =7 TeV*, Phys. Rev. Lett. 106 (2011) 011801

[30] Kraan A. C.: *Interactions of Heavy Stable Hadronizing Particles*, University of Copenhagen, April 2004, arXiv:hep-ex/0404001v1

[31] Kraan A. C., Hansen J.B., Nevski P.: *Discovery potential of R–hadrons with the ATLAS detector*, December 2006, arXiv:hep-ex/0511014v3

[32] ATLAS collaboration: *Search for heavy long-lived charged particles with the ATLAS detector in pp collisions at $\sqrt{s}$ =7 TeV*, Physics Letters B 703 (2011) 428–446

[33] ATLAS collaboration: *Search for stable hadronising squarks and gluinos with the ATLAS experiment at the LHC*, CERN-PH-EP-2011-026

[34] Ohm C.: *Searches for exotic stable massive particles with the ATLAS experiment*, CERN-THESIS-2011-151